République Algérienne Démocratique et Populaire

Ministère de l'Enseignement Supérieur et de la Recherche Scientifique



Ecole Nationale Polytechnique





Département de Génie Mécanique

Final year project thesis for the degree of state engineer in Mechanical Engineering

Development of hydrogen solid storage tank: Numerical investigation of solid-state process and design considerations

TELDJIA Isra

Jury members:

President	M. Mohamed BENBRAIKA	MAA	ENP
Supervisor	M. Arezki SMAILI	Professor	ENP
Co-Supervisor	M. Abdelhamid BOUHELAL	MCA	ENP
Examiner	M. Charafedine BENSACI	MCB	ENP

République Algérienne Démocratique et Populaire Ministère de l'Enseignement Supérieur et de la Recherche Scientifique



Ecole Nationale Polytechnique





Département de Génie Mécanique

Final year project thesis for the degree of state engineer in Mechanical Engineering

Development of hydrogen solid storage tank: Numerical investigation of solid-state process and design considerations

TELDJIA Isra

Jury members:

President	M. Mohamed BENBRAIKA	MAA	ENP
Supervisor	M. Arezki SMAILI	Professor	ENP
Co-Supervisor	M. Abdelhamid BOUHELAL	MCA	ENP
Examiner	M. Charafedine BENSACI	MCB	ENP

République Algérienne Démocratique et Populaire

Ministère de l'Enseignement Supérieur et de la Recherche Scientifique



Ecole Nationale Polytechnique





Département de Génie Mécanique

Mémoire de projet de fin d'études pour l'obtention du diplôme d'ingénieur d'état en Génie Mécanique

Développement d'un réservoir de stockage solide d'hydrogène : étude numérique du procédé à l'état solide et considérations de conception

TELDJIA Isra

Composition du jury :

Président	M. Mohamed BENBRAIKA	MAA	ENP
Encadrant	M. Arezki SMAILI	Professeur	ENP
Co- Encadrant	M. Abdelhamid BOUHELAL	MCA	ENP
Examinateur	M. Charafedine BENSACI	MCB	ENP

ملخص

يعرض هذا العمل دراسة رقمية لتخزين الهيدروجين الصلب في خزانات تعتمد على الهيدريدات المعدنية باستخدام برنامج COMSOL وتركز الدراسة على تقييم تأثير تغيير كتلة المادة الممتصة (الهيدريد المعدني) وحجم الغاز . مبادل الحرارة (السوائل الناقلة للحرارة) على السلوك الحراري وأداء النظام أثناء عملية امتصاص Multiphysics مبادل الحرارة والمعادلات LaNis الهيدروجين. تم اختيار مادة انتقال الحرارة والكتلة لدراسة توزيع درجات الحرارة، ومعدلات الامتصاص، وسعة التخزين في تكوينات مختلفة. وتبين النتائج أهمية تحسين هندسة الخزان وكفاءة التبريد لتحسين أداء التخزين وفقًا لنوع الاستخدام

الكلمات المفتاحية:

تخزين الهيدروجين الصلب، الهيدريدات المعدنية، التحليل الحراري ،تقنية الامتصاص، المحاكاة العددية.

Résumé

Ce travail propose une étude numérique du stockage d'hydrogène solide dans des réservoirs à hydrures métalliques à l'aide du logiciel COMSOL Multiphysics. L'objectif est d'analyser l'impact de la masse d'hydrure métallique et du volume de refroidissement sur le comportement thermique et les performances du système lors du processus d'absorption de l'hydrogène. Le matériau utilisé, LaNis, est modélisé comme un milieu poreux avec ses propriétés thermophysiques spécifiques. Les équations de transfert de chaleur et de masse sont résolues afin d'évaluer la distribution de température, les taux d'absorption et la capacité de stockage pour différentes configurations. Les résultats montrent l'importance d'optimiser la géométrie du réservoir et l'efficacité du refroidissement selon l'application visée.

Mots-clés : Stockage solid d'hydrogène, Hydrure métallique, Analyse thermique, Processus d'absorption, Simulation numérique

Abstract

This work presents a numerical investigation of solid hydrogen storage in metal hydride tanks using COMSOL Multiphysics software. The study focuses on evaluating the influence of varying the metal hydride mass and the cooling volume (heat transfer fluid – HTF) on the thermal behavior and performance of the system during the hydrogen absorption process. The chosen material, LaNis, is modeled as a porous medium with its specific thermophysical properties. The governing equations of heat and mass transfer are solved to analyze temperature distribution, absorption rates, and storage capacity under different configurations. The results highlight the importance of optimizing tank geometry and cooling efficiency to enhance hydrogen storage performance depending on the intended application.

Keywords: Solid hydrogen storage, Metal hydride, Thermal analysis, Absorption process, Numerical simulation.

Dedication

To my beloved parents,

Zouhir and Hanifa,

your endless support, sacrifices, and unconditional love have been the foundation of my journey. This work is a tribute to your strength and unwavering belief in me.

To my dear sisters,

Acinette and Mouna, my beautiful big sister,

thank you for your love, kindness, and encouragement.

To your wonderful children, **Meyssem** and **Jawed**, your smiles have been a source of joy and light throughout this path.

To my brothers, for always being there with silent but meaningful support.

To my loyal friends,

Douaa, Boutheina, Hibet, and Loujain,

thank you for your sincere friendship, constant encouragement, and faith in me.

And most specially, to Mr. Louati Mohammed Fahd,

whose continuous support, valuable guidance, and remarkable dedication have marked this academic year. Your presence, kindness, and wise counsel have truly made a difference. I am deeply thankful for the motivation and clarity you have provided along the way.

Acknowledgments

First and foremost, I would like to express my sincere gratitude to my supervisors, **Arezki Smaili** and **Abdelhamid Bouhelal**, for their continuous guidance, technical support, and valuable feedback throughout the course of this project. Their commitment and expertise were essential in achieving the results presented in this work.

I am also thankful to **Mohamed BENBRAIKA** and **Charafeddine BENSACI** for accepting to assess this work and for their constructive remarks.

My gratitude extends to all **the Mechanical Engineering Department**, whose teachings have shaped my knowledge and skills over the years. Thank you for your dedication and for inspiring us to pursue excellence.

Finally, I would like to thank all those who, in one way or another, have contributed to the completion of this project.

Table of content

I. List of figu	ires	
II. List of tab	oles	
III. Nomencl	ature	
General Intr	oduction	14
Chapter 1: B	ackground of Hydrogen solid storage	17
1.1. Hy	drogen as an energy source	18
1.1.1.	Generalities	18
1.1.2.	Hydrogen characteristics	19
1.2. Hy	drogen production	19
1.2.1.	Electrolysis	19
1.2.2.	Thermochemical Cycles	20
1.2.3.	Direct Thermal Decomposition of Water (Thermolysis)	21
1.2.4.	Photolysis	21
1.2.5.	Hydrogen Production from Biomass	21
1.3. Hy	drogen Storing principal methods	22
1.3.1.	Gaseous Hydrogen Storage	22
1.3.2.	Liquid Hydrogen Storage	22
1.3.3.	Hydrogen solid-state Storage	23
1.4. Hy	drogen solid-state storage materials	23
1.4.1.	Metal Hydrides	24
1.4.2.	Carbon-Based Materials	25
1.4.3.	Metal-Organic Frameworks (MOFs)	25
1.5. MH	I reactors	26
1.5.1.	Metal Hydride Bed Modification	26
1.5.2.	Heat exchangers	28
2. Chapter	2: Bed reactor properties	30
2.1. Pro	perties of the MH bed	31
2.1.1.	Metal hydride basics	31
2.2. The	e material choosing criteria	32
2.2.1.	Magnesium hydride (MgH2)	32

2.2.2.	Titanium iron (TiFe)
2.2.3.	Titanium Dimanganese (TiMn2)
2.2.4.	lanthanum pentanickel (LaNi5)
2.2.5.	sodium aluminum hydride (NaAlH4)
2.2.6.	lithium borohydride (LiBH4)34
2.3. Co	mparative criteria35
2.4. La	Ni5 equations
2.4.1.	Mass and energy conservation
2.4.2.	Specific heat
2.4.3.	MH expansion
2.4.4.	Effective thermal conductivity
2.4.5.	Rate of reaction
2.4.6.	Porosity
2.4.7.	Gas velocity
2.4.8.	Equilibrium pressure
2.4.9.	Heat transfer coefficient
3. Chapter	3: Mathematical model and Numerical method 41
3.1. Sin	nulation model42
3.1.1.	Model definition
3.1.2.	Fluid flow
3.1.3.	Mass transfer
3.1.4.	Heat transfer
3.2. Ch	osen characteristics
3.2.1.	Geometry selection
3.2.2.	Input parameters
3.3. CC	OMSOL Multiphysics interface
3.3.1.	Meshing
3.3.2.	Physics used in simulating absorption
3.3.3.	Studies conducted
3.4. Tir	ne dependent solver
3.5. Ma	iterials definition
4. Chapter	4: Results and discussions 53

4.1. Res	sults obtained from simulation	54
4.1.1.	Mesh dependency	54
4.1.2.	Absorbed hydrogen content	55
4.1.3.	Hydrogen mass profile	55
4.1.4.	Evolution of Hydrogen content over time	56
4.1.5.	Pressure Evolution	57
4.2. Inv	restigation of the simulation results validity	58
4.2.1.	Comparative analysis with experimental results	58
4.2.2.	Investigation of mesh dependency	60
4.3. Siz	ing study	60
4.3.1.	Simulation Data from COMSOL	61
General con	clusion	63
Bibliography	у	65

I . List of figures

I. List of figures

Figure 1 Hydrogen production and applications	18
Figure 2 Schematic diagram of alkaline water electrolysis hydrogen production device	. 20
Figure 3 Hydrogen Production by Solar Thermochemical Water-Splitting Cycle via a Beam	
Down Concentrator	. 20
Figure 4 Schematic of a direct photolysis process	. 21
Figure 5 Representation of different hydrogen storing methods	. 22
Figure 6 Schematic of Hydrogen absorption/desorption process in a metal hydride	. 24
Figure 7 Hydrogen storage carbonaceous materials	. 25
Figure 8 Current trends in potential use of MOFs for hydrogen storage	25
Figure 9 Metal hydride reactor shapes, thermal performance enhancement methods and	
proposed solutions	. 26
Figure 10 Effect of different reactors (a) and fin configuration (b) on the bed temperature $lpha$	and
hydrogen concentration	. 28
Figure 11 Three different configurations of annular metal hydride reactor	. 29
Figure 12 Influence of fin number (a) and fin thickness (b) on hydrogen absorption rate $$	29
Figure 13 a) Ideal PCI at different temperatures with the corresponding b) van't Hoff plot $lpha$	and
c) real PCI with hysteresis and plateau slope	31
Figure 14 Van't Hoff's plots of alloys type AB	. 32
Figure 15 Van't Hoff's plots of alloys type AB2	33
Figure 16 Van't Hoff's plots of alloys type AB5	. 34
Figure 17 The studied model illustration	. 42
Figure 18 Illustration of 5/8 of the tank geometry without hydride alloy	. 43
Figure 19 Illustration of the meshs conducted	. 49
Figure 20 Meshing example interface	50
Figure 21 The physics used interface	. 50
Figure 22 The studies conducted interface	51
Figure 23 Illsutration of the solver interface	52
Figure 24 Illustration of the materials selection interface	52
Figure 25 The studied models with different alloy mass	. 60
Figure 26 Hydrogen content and temperature distribution	55
Figure 27 Plots of the hydrogen influx, adsorbed and mass change	. 56
Figure 28 Plots of XH, Hydride and Gas temperature	. 56
Figure 29 Pressure and Temperature evolution over time	57

II. List of tables

Table 1 Hydrogen caracteristics	19
Table 2 the metal hydride bed alteration techniques	27
Table 3 Advantages and disadvantages of hydrides	35
Table 4 The model's geometry parameters	47
Table 5 Input parameters of the simulation model	49
Table 6 The models kinetic parameters	49
Table 7 Table showing the meshing conducted with CPU time and absorbed mass of H2	54
Table 8 Key results obtained from simulation	58
Table 9 Key results obtained from the experimental study	59
Table 10 Mesh dependency of the published model	60
Table 11 Simulations obtained data	61

Ⅲ. Nomenclature

III. Nomenclature

The main nomenclature used in this report is listed below. Additional symbols and notations are introduced and explained throughout the report as needed.

X	Hydrogen-to-metal atomic ratio	
W	Amount of hydrogen taken up	
F	Reacted fraction	
3	Porosity	
ρ	Density	Kg/m^3
C_p	Specific heat capacity	J/kg.K
k	Thermal conductivity	W/m.K
μ	Dynamic viscosity	Pa.s
ΔH	Enthalpy change	J/mol
E_a	Activation energy	J/mol
C_a	Pre-exponential factor	1/s
P	Pressure	Pa, atm
T	Temperature	K
N	Particle coordination number	
V	~ ~ 1 1 21 1 1	
	Superficial flow velocity	m/s
K	Superficial flow velocity Permeability	m/s m^2
	•	
K	Permeability	
K Re	Permeability Reynolds number	
K Re Pr	Permeability Reynolds number Prandtl number	
K Re Pr Nu	Permeability Reynolds number Prandtl number Nusselt number	m^2

Abbreviation

MH	Metal hydride
HTF	Heat Transfer Fluid
MOF	Metal-Organic Framework
PCI	Pressure Composition Isotherm
LHV	Lower heating value
ENG	Expanded Natural Graphite
BDF	Backward Differentiation Formula

General Introduction

The increasing demand for clean and sustainable energy sources has driven significant interest in hydrogen as an energy carrier. Hydrogen presents a promising solution to global energy challenges, particularly as an alternative to fossil fuels, which contribute to greenhouse gas emissions and environmental degradation. Among various hydrogen storage methods, solid-state storage through absorption in metal hydrides or other solid materials offers advantages in terms of safety, efficiency, and energy density. However, the development of a practical and efficient solid hydrogen storage tank involves numerous technical and engineering challenges.

This project focuses on the development of a hydrogen solid storage tank, emphasizing the numerical investigation of the solid-state process and design considerations. The primary objective is to design a storage system that effectively utilizes the absorption and desorption process in a solid material, ensuring optimal hydrogen storage capacity, thermal management, and structural integrity. To achieve this, the study follows a structured approach addressing fundamental aspects of the tank's design and operation.

The first step involves identifying suitable materials for hydrogen storage. A comprehensive literature review will be conducted to examine potential materials based on their absorption properties, reaction kinetics, thermal behavior, and overall feasibility for practical applications. This selection process will establish a foundation for the subsequent design phase.

The next stage focuses on reconstituting a design of the hydrogen storage tank. A simplified analytical model has been developed to highlight critical design parameters governing storage capacity and thermal performance. This model will provide insights into the fundamental principles influencing the tank's operation. Subsequently, a more detailed mathematical model will be formulated to incorporate the complex physical processes involved in the absorption cycle. Numerical simulations have been employed to refine the design and ensure optimal hydrogen mass capacity under various operational conditions.

A structured approach has been adopted throughout this study to investigate and optimize solidstate hydrogen storage using metal hydrides, with a strong focus on thermal management and numerical modeling.

Chapter 1 presents generalities about hydrogen, including its physical and chemical properties, its role in the energy transition, and the various methods available for its storage. Special attention is given to solid-state storage using metal hydrides, as well as an overview of commonly used materials, and the importance of thermal management systems, such as heat exchangers, in hydrogen storage applications.

Chapter 2 introduces the mathematical modeling of the absorption process. It discusses the selection of the working material (metal hydride) based on its capacity, thermodynamic behavior, and suitability for solid storage. The governing equations of mass and energy transfer that describe the hydrogen absorption process are detailed and justified based on the physical phenomena involved.

General Introduction

Chapter 3 focuses on the numerical modeling phase, where simulations were conducted using COMSOL Multiphysics to analyze the thermal and storage performance of the system under different reactor configurations. These configurations vary in terms of metal hydride mass and cooling system volume, allowing for a comparative analysis of their impact on heat distribution, absorption rates, and overall system efficiency. A mesh dependency study has been conducted.

Chapter 4 aim to show results of the simulations and the focus on the aspect of meshing, also a comparison between a real experiment of a metal hydride reactor to prove the validity of the results obtained in the simulation.

Finally, a general conclusion overall the work conducted.

Through this multi-step methodology, the research aims to contribute valuable insights into material selection, heat exchanger integration, and numerical analysis, supporting the development of efficient, compact, and scalable hydrogen storage solutions. These findings are relevant not only for stationary applications but also for mobile and transport systems, thereby contributing to the broader goals of renewable energy deployment and decarbonization of the energy sector.

Chapter 1 Background of Hydrogen solid storage

1.1. Hydrogen as an energy source

1.1.1. Generalities

One intriguing alternative energy source is hydrogen. Hydrogen energy has been utilized in fuel cell cars, the defense sector, and aviation and aerospace over the past century. Because of its high calorific value and lack of adverse environmental effects, hydrogen has emerged as a viable alternative in this regard. However, there are a number of challenges associated with the deployment of a hydrogen energy system because it is a big and intricate technical system that involves the generation, storage, and usage of hydrogen. Implementing safe and effective hydrogen storage and transportation is one of the main obstacles to large-scale hydrogen uses. However, hydrogen storage is a significant issue that restricts the utilization of hydrogen. [1]

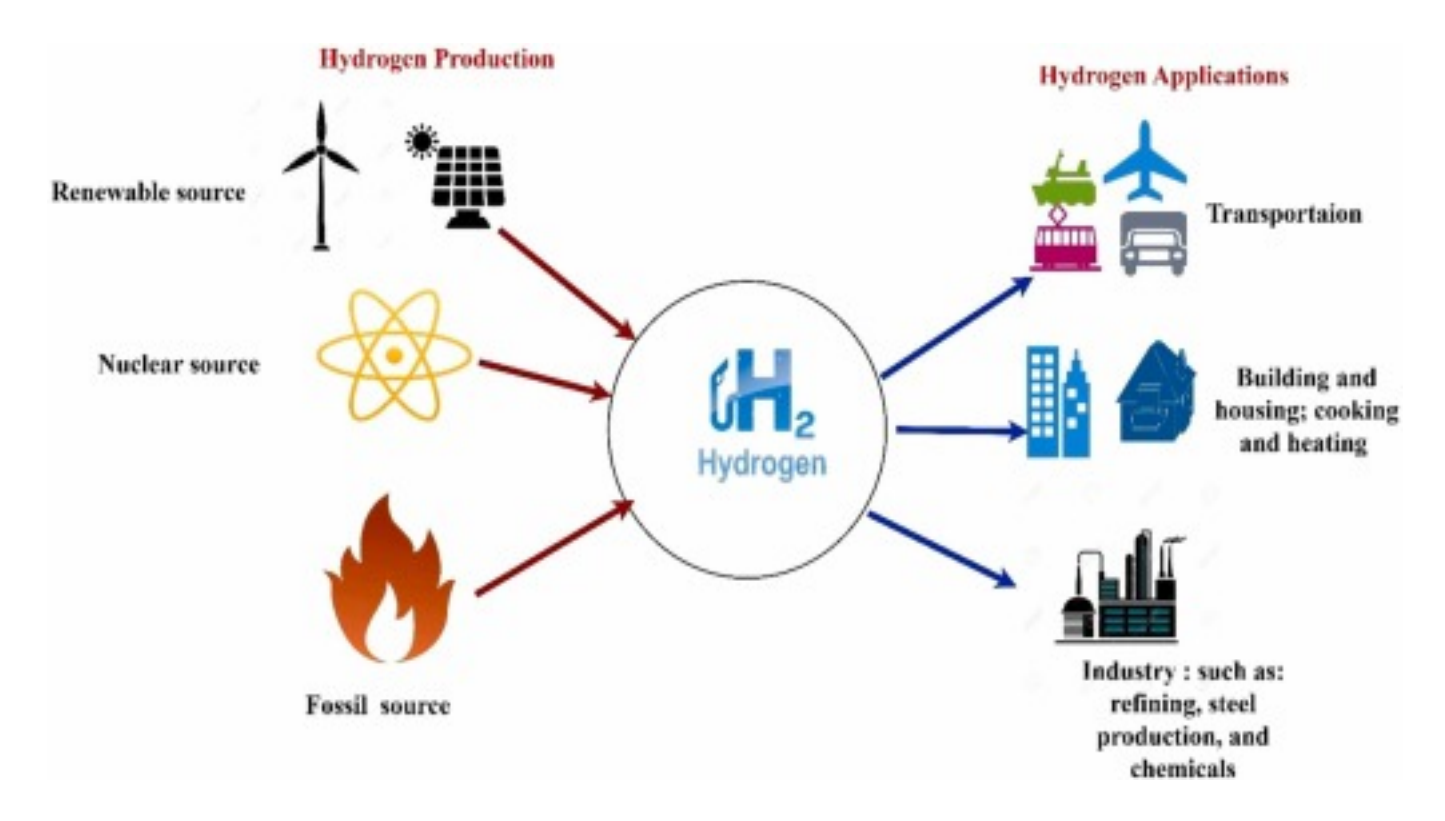


Figure 1 Hydrogen production and applications [12]

In addition to the technical challenges, the economic viability of hydrogen energy remains a key factor in its widespread adoption. The costs associated with hydrogen production, infrastructure development, and storage technologies are still relatively high compared to conventional fossil fuels. Moreover, building a comprehensive hydrogen supply chain—from generation facilities to refueling stations—requires substantial investment and long-term policy support. Nevertheless, as countries seek to decarbonize their energy sectors and reduce dependence on imported fuels, hydrogen is increasingly seen as a strategic energy carrier that can contribute to energy security, job creation, and the development of a low-carbon economy.

1.1.2. Hydrogen characteristics

The most prevalent isotope of the lightest element, the hydrogen atom, has just one proton and one electron. H2 molecules, which are smaller than most other molecules, are easily formed by hydrogen atoms. Colorless, odorless, and tasteless, the molecular form of hydrogen is roughly 14 times lighter than air and diffuses more quickly than any other gas. Hydrogen condenses to a liquid at -253°C and a solid at -259°C when it cools. Table 1.1 provides a summary of hydrogen's physical characteristics. The density of ordinary hydrogen is 0.09 kg/m3. It is therefore the lightest material known, buoyant in air at 1.2 kg/m3. Compared to

other solid elements, solid metallic hydrogen has the highest electrical conductivity. Also, the gaseous hydrogen has one of the highest heats capacities (14.3kJ/kg.K).

Property	Value
Molecular weight	2.01594
Density of gas at 0°C and 1 atm	0.08987 kg/m³
Density of solid at −259°C	858 kg/m³
Density of liquid at −253°C	708 kg/m ³
Melting temperature	−259°C
Boiling temperature at 1 atm	−253°C
Critical temperature	-240°C
Critical pressure	12.8 atm
Critical density	31.2 kg/m³
Heat of fusion at −259°C	58 kJ/kg
Heat of vaporization at −253°C	447 kJ/kg
Thermal conductivity at 25°C	0.019 W/(m·°C)
Viscosity at 25°C	0.0892 centipoise
Heat capacity (Cp) of gas at 25°C	14.3 kJ/(kg·°C)
Heat capacity (Cp) of liquid at −256°C	8.1 kJ/(kg·°C)
Heat capacity (Cp) of solid at −259°C	2.6 kJ/(kg·°C)

Table 1 Hydrogen caracteristics [3]

1.2. Hydrogen production

In crustal reserves, hydrogen is typically present in trace amounts along with natural gas. Nonetheless, some wells have been discovered to have high hydrogen contents. For example, some wells in Kansas have 40% hydrogen, 60% nitrogen, and trace levels of hydrocarbons [3]. The most logical source for large-scale hydrogen production is water. Methods of hydrogen production from water include electrolysis, direct thermal decomposition or thermolysis, thermochemical processes, and photolysis.

1.2.1. Electrolysis

Water electrolysis is a well-established technology that produces hydrogen using a fundamentally straightforward method. It is very effective and devoid of moving parts. It works well for producing hydrogen on a huge scale. Efficiency ranges from 72% to 82% on average. There are a number of cutting-edge electrolysis technologies under development, including

Chapter 1: Background of Hydrogen solid storage

advanced alkaline electrolysis, which uses novel membrane and electrode materials to further increase efficiency—up to 90% [4, 5].

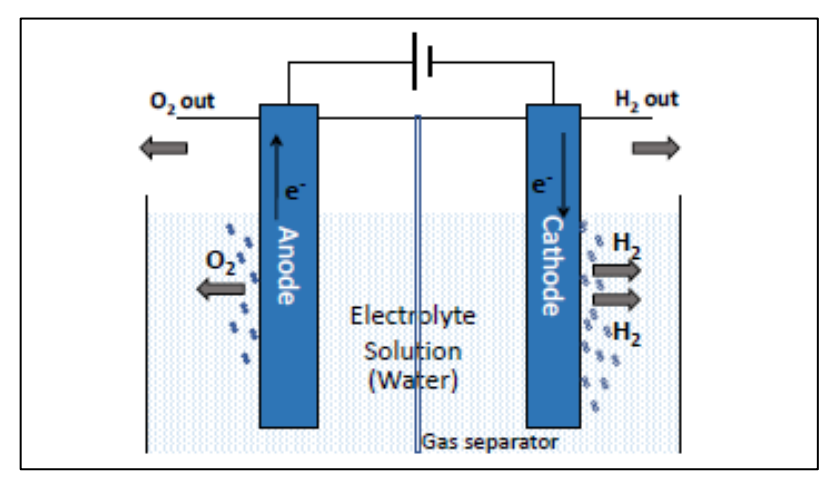


Figure 2 Schematic diagram of alkaline water electrolysis hydrogen production device [18]

1.2.2. Thermochemical Cycles

When hydrogen is produced using thermochemical cycles, water is chemically divided at temperatures lower than those required for thermolysis, resulting in a sequence of cyclical chemical processes that eventually liberate hydrogen. Sulfuric acid—iodine, hybrid sulfuric acid, hybrid sulfuric acid—hydrogen bromide, calcium bromide—iron oxide (UT-3), and iron—chlorine cycles are some of the more extensively studied thermochemical process cycles. The efficiencies that can be achieved range from 40% to 50%, depending on the temperatures at which these processes are taking place. However, for these approaches to be practical, issues with corrosion at high temperatures, toxicity of some of the chemicals involved, and the movement of enormous masses of materials in chemical reactions need to be resolved [6, 7, 8].

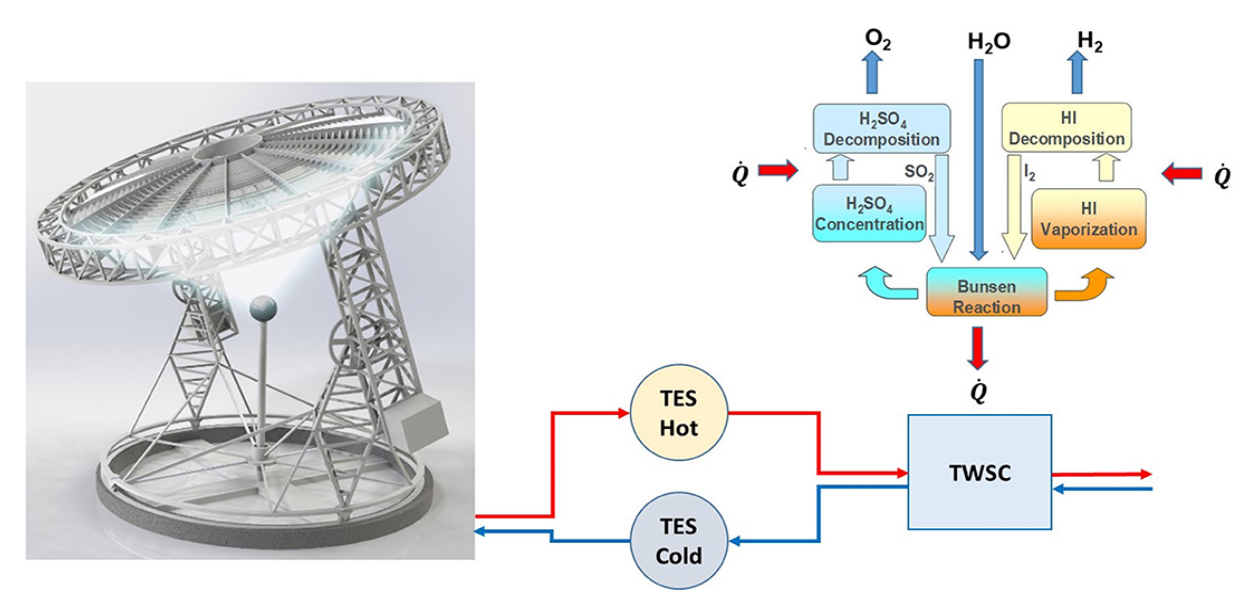


Figure 3 Hydrogen Production by Solar Thermochemical Water-Splitting Cycle via a Beam Down Concentrator [3]

1.2.3. Direct Thermal Decomposition of Water (Thermolysis)

At temperatures higher than 2000 K, thermal splitting of water is possible. Temperature affects the degree of dissociation, which is just 1% at 2000 K, 8.5% at 2500 K, and 34% at 3000 K. At very high temperatures, the result is a combination of gases. The primary issues with this approach are the materials needed for extremely high temperatures, the high-temperature recombination of reaction products, and the separation of hydrogen from the mixture [9].

1.2.4. Photolysis

Photolysis (or direct extraction of hydrogen from water using only sunlight as an energy source) can be accomplished by employing photobiological systems, photochemical assemblies, or photoelectrochemical cells. Intensive research activities are opening new perspectives for photoconversion, where new redox catalysts, colloidal semiconductors, immobilized enzymes, and selected microorganisms could provide means of large-scale solar energy harvesting and conversion into hydrogen [10, 11].

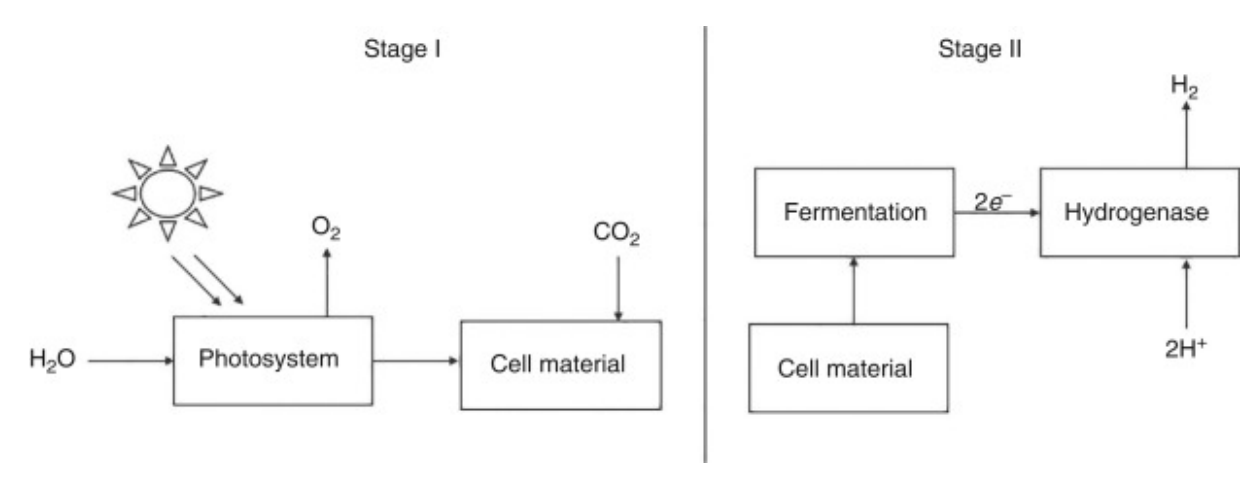


Figure 4 Schematic of a direct photolysis process [8]

1.2.5. Hydrogen Production from Biomass

A pyrolysis/gasification method can be used to produce hydrogen from biomass. In the biomass preparation process, the biomass/water slurry is heated in a reactor to high temperatures while under pressure. The biomass is broken down and partially oxidized during this process, resulting in a gas product that includes CO2, CO, nitrogen, methane, and hydrogen. The reactor's bottom is cleared of mineral debris. The hydrogen content of the gas stream is raised in a high-temperature shift reactor. The next pressure swing adsorption unit produces relatively high-purity hydrogen. Except for the reactor architecture and the biomass pretreatment unit, the entire system is remarkably similar to a coal gasification plant. Due to biomass's decreased calorific value per mass unit as compared to coal, the processing facility is larger than that of a comparably sized coal gasification plant [12].

1.3. Hydrogen Storing principal methods

The storage of hydrogen fuel can be accomplished in three different ways, each with pros and cons. Compressing and storing the hydrogen gas in a high-pressure cylinder is the first technique. A three-layer aluminum, carbon fiber, and glass fiber tank that can store hydrogen at pressures as high as 350 atm (~35,000 kPa) is currently used in the Honda FCX vehicle. [1]. Cryogenically liquefying the hydrogen and storing it in a dewar in liquid form is an additional technique. The condensation point of hydrogen is around 20 K (~-253°C) at 1 atm (~100 kPa). (~-253°C) [13]. Having the hydrogen absorbed into a metal alloy is the third method of solid-state storage. The majority of metals and alloys can reversibly absorb hydrogen; when this occurs, the metal or alloy is referred to as a metal hydride.

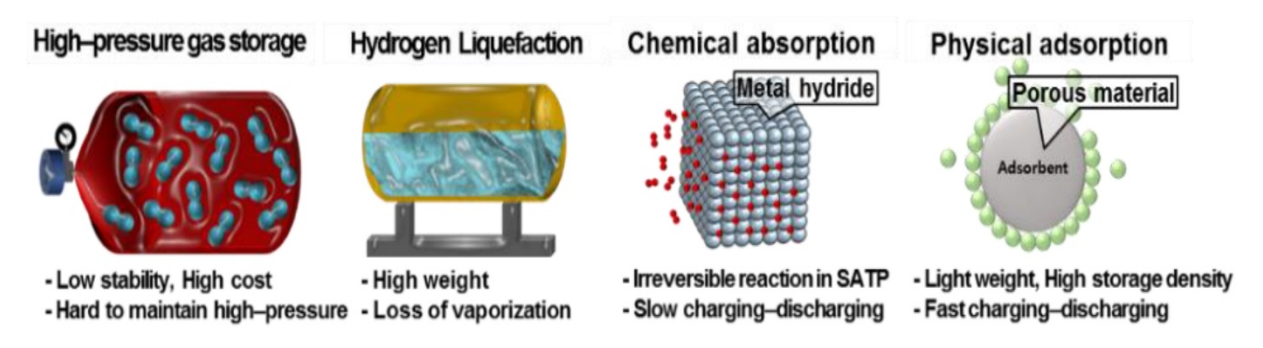


Figure 5 Representation of different hydrogen storing methods [18]

1.3.1. Gaseous Hydrogen Storage

There may be a variety of hydrogen storage system types available, depending on the use and storage size. This includes vehicle tanks to store hydrogen used as fuel for road vehicles; stationary large storage systems and stationary small storage systems at the distribution or final user level; and mobile storage systems for transport and distribution, including both small systems (like a gaseous or liquid hydrogen truck trailer) and large-capacity devices (like a liquid hydrogen tanker—bulk carrier). Since hydrogen has a low density, it must constantly be stored in relatively large volumes and is linked to either very low temperatures or high pressures, which necessitate the use of heavy vessels, or it must be combined with other materials, which are considerably heavier than hydrogen. Research on massive subterranean hydrogen storage [13] [14]. Pressurized gas storage systems come in a variety of sizes and pressure ranges, including permanent high-pressure containers (over 200 bar), low-pressure spherical containers (>30,000 m3, 12-16 bar), and standard pressure cylinders (50 L, 200bar) [15].

1.3.2. Liquid Hydrogen Storage

The advantages of liquid hydrogen include its high specific heat and high heating value per unit mass, which allow it to cool down significantly [16]. There are several significant applications for liquid hydrogen, including bubble chambers, high-energy nuclear physics, and the space program. Despite the need for specific Dewar vessels and cryogenic cooling, transporting hydrogen in liquid form is far more cost-effective. Although there are many benefits to liquid

Chapter 1: Background of Hydrogen solid storage

hydrogen, its applications are limited in part due to the high energy consumption (about 30% of its heating value) associated with liquefying hydrogen using current conventional methods. A medium-sized plant needs 10–13 kWh of energy (electricity) to liquefy 1 kilogram of hydrogen [17]. Furthermore, up to 40% of liquid hydrogen's available combustion energy may be lost due to boil-off losses during handling, storage, and transit. Therefore, it's critical to look for methods to increase the liquefiers' efficiency and reduce boil-off losses.

1.3.3. Hydrogen solid-state Storage

Hydrogen can create metal hydrides when certain metals and alloys are present. Hydrogen atoms are injected into gaps inside the metal or alloy's lattice as a result of the splitting of hydrogen molecules. This produces efficient storage with a density similar to that of liquid hydrogen. Nevertheless, the metal hydride gravimetric storage density is comparable to that of pressurized hydrogen storage when the mass of the metal or alloy is considered. For a high-temperature hydride like MgH2, the optimal possible gravimetric storage density is roughly 0.07 kg of H2/kg of metal [18]. Heat is released throughout the storage process (charging or absorption), and this heat needs to be eliminated to ensure the reaction continues. Heat must be provided to the storage tank during the hydrogen release process, also known as desorption or discharge. The safety factor is one benefit of storing hydrogen in hydriding materials. Since hydrogen would stay in the metal structure, a hydride tank that sustains significant damage (like that which might result from a collision) would not be a fire threat.

Criteria that are expected for selection of solid-state hydrogen storage systems are resumed as follows:

- > Favorable thermodynamics.
- > Fast adsorption-desorption kinetics.
- Large extent of storage (high volumetric and gravimetric density).
- Withstand enough cycle number for both adsorption and desorption.
- > Enough mechanical strength and durability.
- > Appropriate heat transfer medium.

1.4. Hydrogen solid-state storage materials

Solid-state hydrogen storage is one solution various challenges. Materials under investigation include organic polymers, metal—organic frameworks (MOFs), composites/hybrids, alloys, and hydrides (metal-, boro-, and complex-), metal oxides and mixed metal oxides, clay and zeolites, and carbon materials (CNT, graphene).

In the passages below we will introduce and detail about the most common used materials among the ones named before.

1.4.1. Metal Hydrides

Metallic hydrides (MHs) are conductive, nonstoichiometric solids that can form with a variety of d- and f-block elements. There have been reports of saline, intermediate, metallic, and molecular binary metal hydrides, but some d-block elements, like iron and ruthenium, do not form binary hydrides. Since the 1970s, several alloys have been designed and formulated as an effective hydrogen storage material, such as AB5, AB3, A2B7, AB2, AB, and A2B. In these compounds, A is an absorbing hydrogen metallic element, and B is a weak hydrogen absorber-based metallic element with high catalytic activities; B is crucial to the hydrogen dissociation process(H2→2H).

In practice, hydrogen storage devices employ a wide range of alloys and MHs. MHs suffer from low gravimetric densities and high enthalpy of formation, despite having significant volumetric densities of about 115 kg/m3 (for the reference material LaNi5 compound). Metal hydrides react with a variety of metals and metal alloys to produce hydrogen. By releasing hydrogen and regenerating the metal or alloy, this process can be undone. Compared to hydrogen physisorption, which is regarded as hydrogen storage, metal hydrides offer a significant advantage. Particularly when the H:M ratio is two or higher, the compounds that contain hydrogen and light elements (such Li, Be, Na, Mg, B, and Al) present interesting materials in this sector. Hydrogen can be incorporated into metals or intermetallic from either an electrolytic solution or from the gaseous phase. [19]

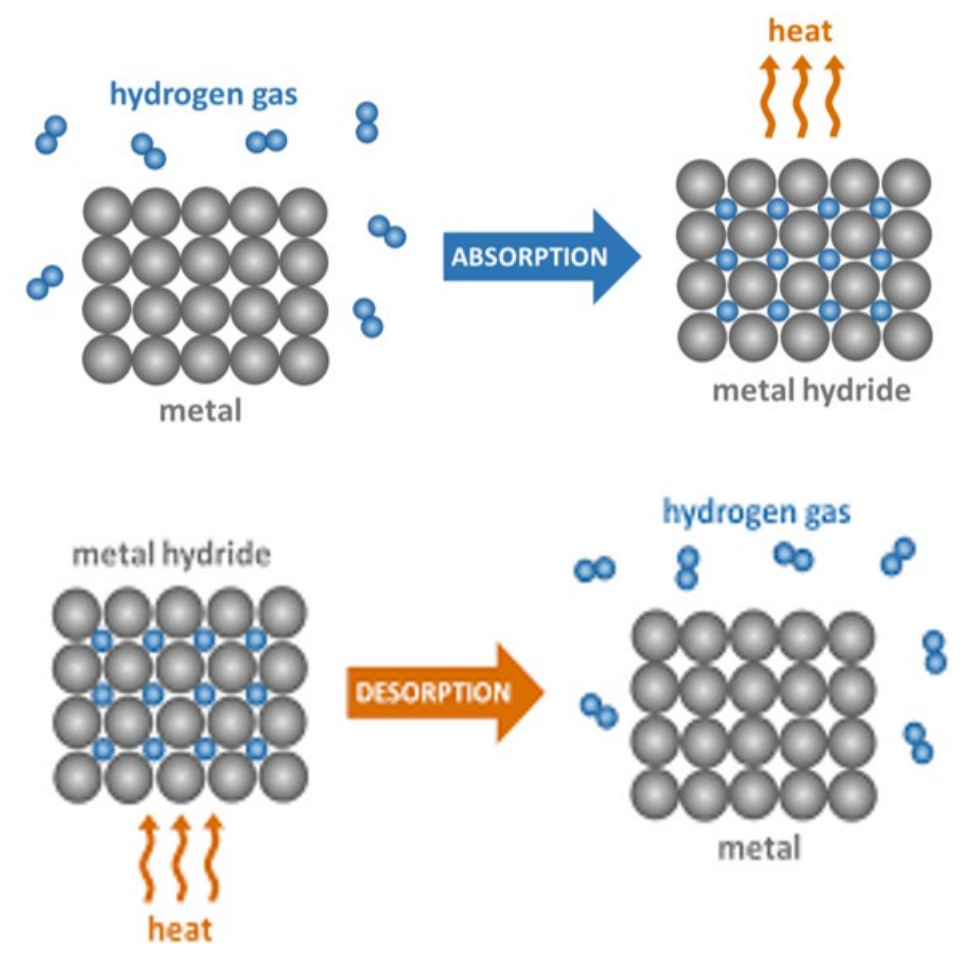


Figure 6 Schematic of Hydrogen absorption/desorption process in a metal hydride [10]

1.4.2. Carbon-Based Materials

The best solid-state host for storing hydrogen is carbon. Because of their high specific surface area, carbon materials represent a broad class of nano-/microporous materials that have been proposed for hydrogen storage. Carbon dots (CDs), graphene (GO), fullerene (F), carbon nanotubes (CNTs), multiwall carbon nanotubes (MWCNTs), and activated carbons (ACs). The Langmuir isotherm model suggests that certain materials can undergo reversible hydrogen sorption. These materials' limited adsorption capacity at high cryogenic and low pressure has limited their vast range of applications. An overview of the hydrogen storage process in carbonaceous materials is presented in the figure 1-7. [20, 21]

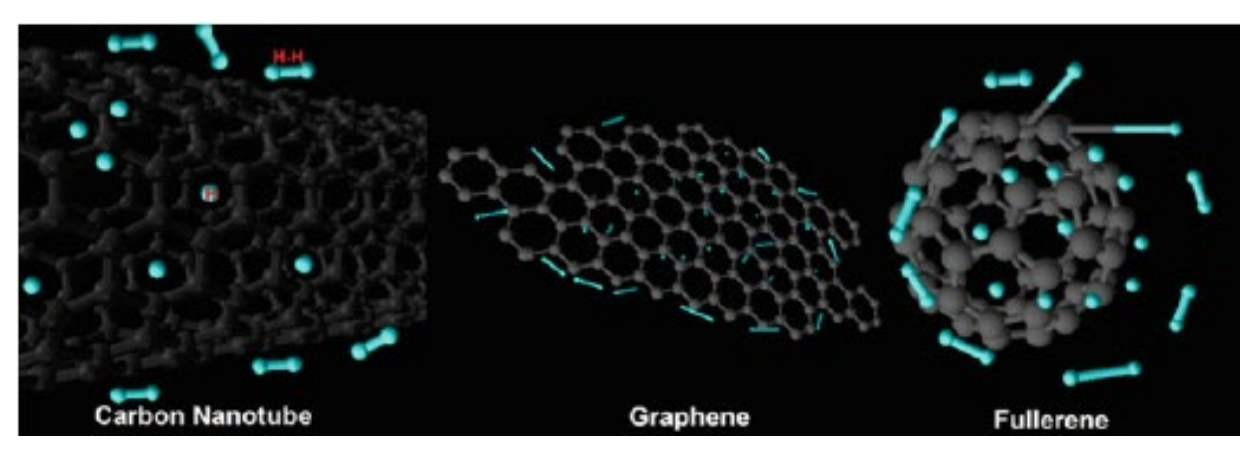


Figure 7 Hydrogen storage carbonaceous materials [2]

1.4.3. Metal-Organic Frameworks (MOFs)

Metal-organic frameworks (MOFs) are made up of metal ions joined by multidentate organic ligands. These materials enormous surface areas, consistent porosity structure, and presence of metallic-core-redox species have earned them the label of "multi-hydrogen absorber. When MOFs are arranged in three dimensions, a network of channels is created. Narrow pores are more effective than broad pores in this class of materials when it comes to harvesting hydrogen absorption at room temperature. There are several types of MOF systems that exhibit structure-performance correlations, including covalent organic frameworks, mixed ligand/functionality systems, carboxylate-based frameworks, and heterocyclic azolate-based frameworks. [19]

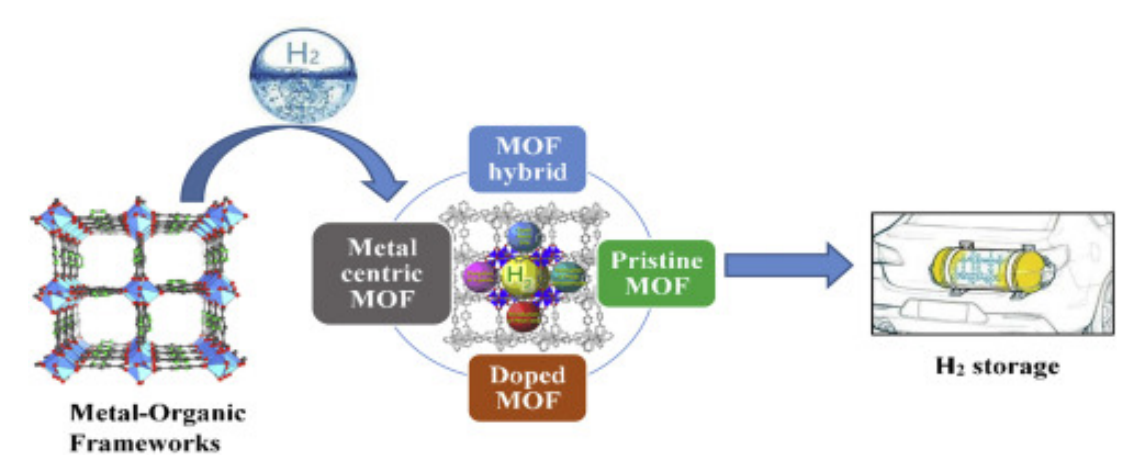


Figure 8 Current trends in potential use of MOFs for hydrogen storage [12]

1.5. MH reactors

A large number of solutions for the problem of poor heat and mass transfer in metal hydride layers have been proposed. The most common method of solving this problem is the use of heat exchange systems inside the reactor. Many scientific papers present mathematical calculations, as well as the results of simulation and design optimization of metal hydride reactors, performed in order to optimize the number of heat exchange elements and determine the best configuration of a metal hydride bed. A large number of review works have also been carried out, in which some thermal management solutions and configurations of metal hydride reactor with heat exchangers were considered [22, 23]. According to the studies carried out, it is possible to sum up the number of reports and articles aimed at solving the problems of heat transfer in metal hydride reactors.

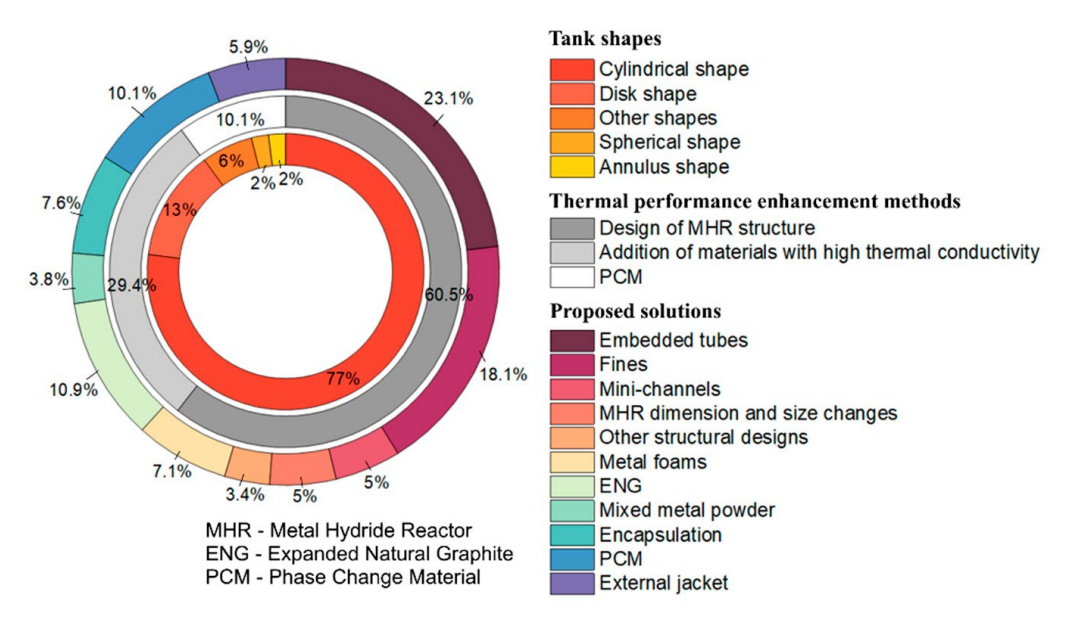


Figure 9 Metal hydride reactor shapes, thermal performance enhancement methods and proposed solutions [49]

Currently, 3D technologies are receiving a lot of attention as well. Additive manufacturing technologies can be used to create high-efficiency heat exchangers designed for installation in metal hydride reactors. Additive manufacturing makes it possible to produce small parts with exceptionally complex shapes, as well as internal structures and matrices that are impossible with any other method of manufacturing. Additively manufactured aluminum heat exchangers already exist and are used in many applications [24, 25].

1.5.1. Metal Hydride Bed Modification

Increasing the contact area between the particles raises the effective heat conductivity. For improved heat conductivity, the metal hydride particles must be crushed, or packed closely together. But even if heat transmission is beneficial, excessive compression significantly reduces the amount of hydrogen that can be stored [26]. However, because loosely packed particle beds have a significantly poorer heat transfer efficiency, compacts are frequently utilized in research. Many studies use metal hydride powder compacts, which are made by pressing hydrogen storage material with additions, to boost the powders' effective thermal conductivity. Ron M. et al. initially suggested this technique using aluminum powder [27], Kim K. J. et al. with copper and tin powder [28] and Klein H. P. et al. with expanded graphite [29].

Chapter 1: Background of Hydrogen solid storage

Even while effective conductivity has significantly increased, the use of foam metals impairs the mass transfer process, reduces the hydrogen storage capacity, and prevents hydrogen from diffusing in the metal hydride layers. Alternative approaches, such as the use of cooling tubes, fins, and external jackets, are being contemplated in this context. The most promising option is to use these heat exchangers, but their design determines their characteristics and how they affect thermal conductivity in the metal hydride layer.

A brief summary of the metal hydride bed alteration techniques under consideration is given in the table below.

Metal Hydride Material	Type of Modification	Heat Transfer Coefficient (W/m·K)
Mn $Ni_{4.15}Fe_{0.85}$	Aluminum foam	6.9
Mn $Ni_{3.6}Al_{0.54}$	Copper wire matrix	0.5–2.5
La $Ni_{4.85}Sn_{0.15}$	Expanded natural graphite flakes	19.5
La <i>Ni</i> ₅	Porous metallic-matrix hydride compacts with aluminum	12.3
La <i>Ni</i> ₅	Copper encapsulation	3.5
La <i>Ni</i> _{4.75} Al0.25	Copper coating	1.78–4.3
La <i>Ni</i> ₅	Aluminum foam	<10.0
La <i>Ni</i> ₅	Copper coating	6.0–9.0
La <i>Ni</i> ₅	Copper encapsulation	2.17–6.6
La <i>Ni</i> ₅	Copper coating	5.0
$Ca_{0.6}Mm_{0.4}Ni_5$	Copper coating	0.8–2.8
$Mg_{90}Ni_{10}$	Pelletized hydride-graphite composites	10.0
Hydralloy® C5-based MHC	Metal hydride/ENG compacts	10–15
$La_{0.8}Ce_{0.2}Ni_5$	Graphite flakes	4.7
$La_{0.8}Ce_{0.2}Ni_5$	Graphite flakes with copper wires	6.8
$La_{0.8}Ce_{0.2}Ni_5$	Metal hydride/ENG compacts	8.1
MgH_2	Metal hydride/ENG compacts	10.4–4.2

Table 2 the metal hydride bed alteration techniques [26]

1.5.2. Heat exchangers

In metal hydride reactors, heat exchangers are frequently used to address heat transfer issues. A specific structure of heat exchange surfaces, like fins, can be chosen and the number of tubes can be optimized thanks to the design of cylindrical reactors. Numerous studies have been conducted in this area on the choice of heat exchanger As a component of the current study on heat exchanger shape optimization, another option would be to employ the U-shaped cooling tubes. Bai X. S. et al. provided a performance comparison of a LaNi5 metal hydride reactor with a finned double U-shaped tube heat exchanger and a finned single tube heat exchanger in their work on simulations [30]. According to the findings, the U-tube type took 1200 seconds to charge, whereas the single-finned tube model took 2800 seconds. With loop-type fins and an exterior heat exchanger, the authors have created a more sophisticated heat exchanger design. Four tubes were employed to provide hydrogen in the reactor model. With a central cooling tube and cooling jacket, circular fins were included into the reactor. Fins were therefore separated into outer fins that were mounted on the side of the water jacket and inner fins that were mounted on the straight tube. Compared to hydride reactors using a single finned tube heat exchanger, the suggested hydride reactor's charging time for achieving 90% hydrogen saturation has been reduced by roughly 57% and 82%.

and, correspondingly, a finned double U-shaped tube heat exchanger. The scientists also examined three other metal hydride reactor configurations: seven with 1 mm thick fins, fourteen with 0.5 mm thick fins, and thirty-five with 0.2 mm thick fins. It was found that the hydrogen absorption reaction rate can be increased by increasing the number of fins with a small thickness.

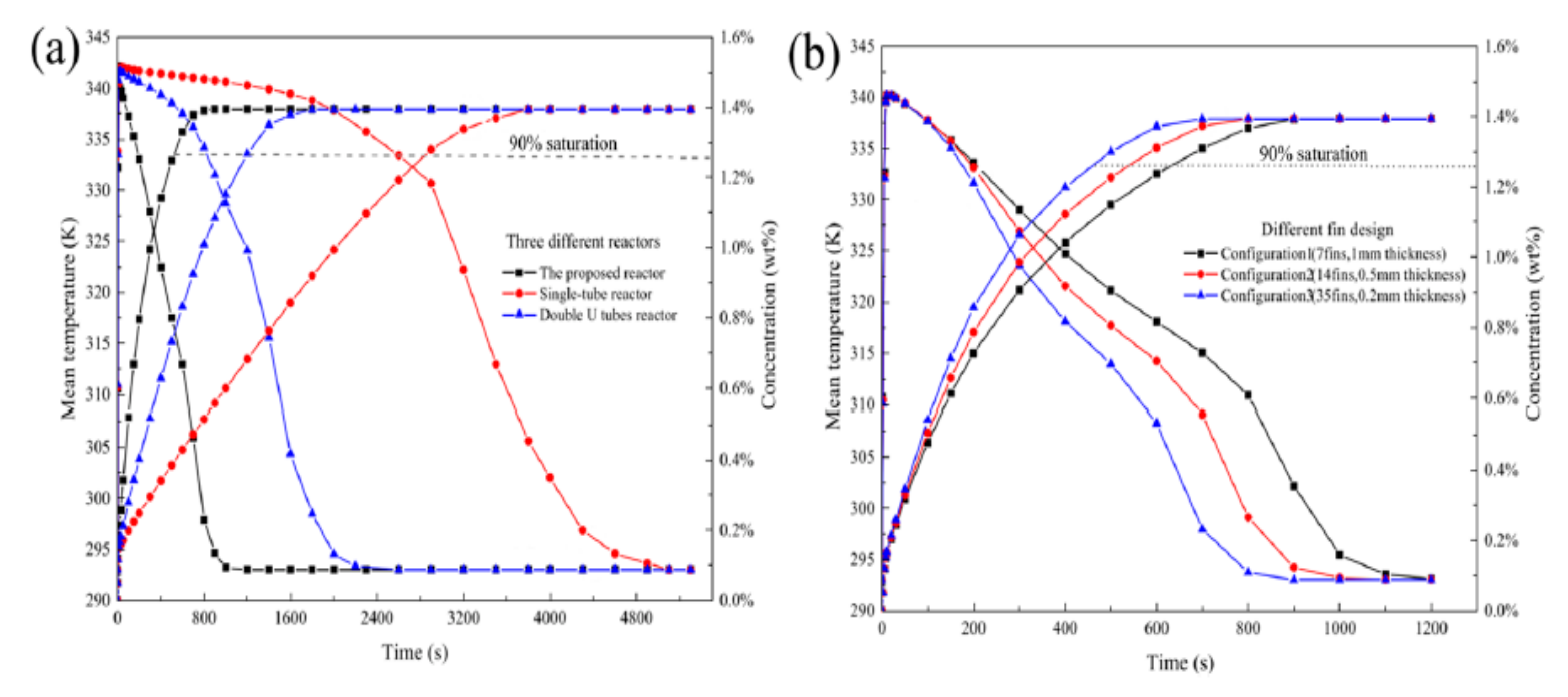


Figure 10 Effect of different reactors (a) and fin configuration (b) on the bed temperature and hydrogen concentration [35]

Chapter 1: Background of Hydrogen solid storage

Prasad J. S. and Muthukumar P. considered three configurations of annular metal hydride reactors. The first configuration and the second configuration differed in the heat transfer fluid's flow direction, and the third configuration was the same as the second, but with the addition of radial fins without any specific geometry [31].

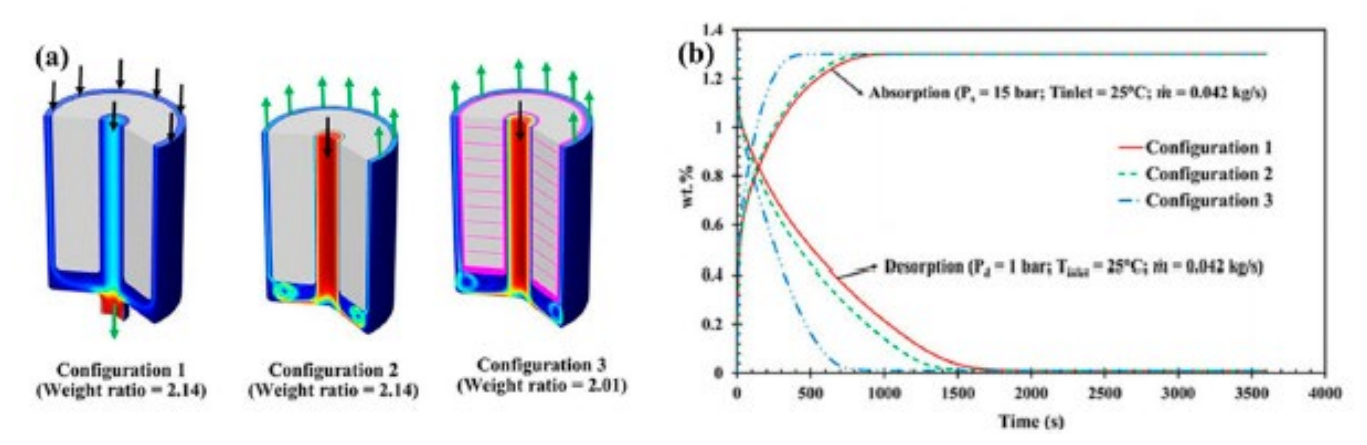


Figure 11 Three different configurations of annular metal hydride reactor [22]

In terms of both absorption and desorption rates, the authors discovered that the second configuration is superior to the first. Nonetheless, there was not much of a difference between the absorption rates for the first and second configurations. Cross fins, which take up only 4.6% of the reactor capacity, significantly increase the rate of hydrogen sorption and desorption.

The scientific literature frequently takes longitudinal fins into consideration in addition to transverse fins. In order to investigate the impact of supply pressure, cold/hot fluid temperature, and total heat transfer coefficient on hydrogen storage capacity, Muthukumar P.

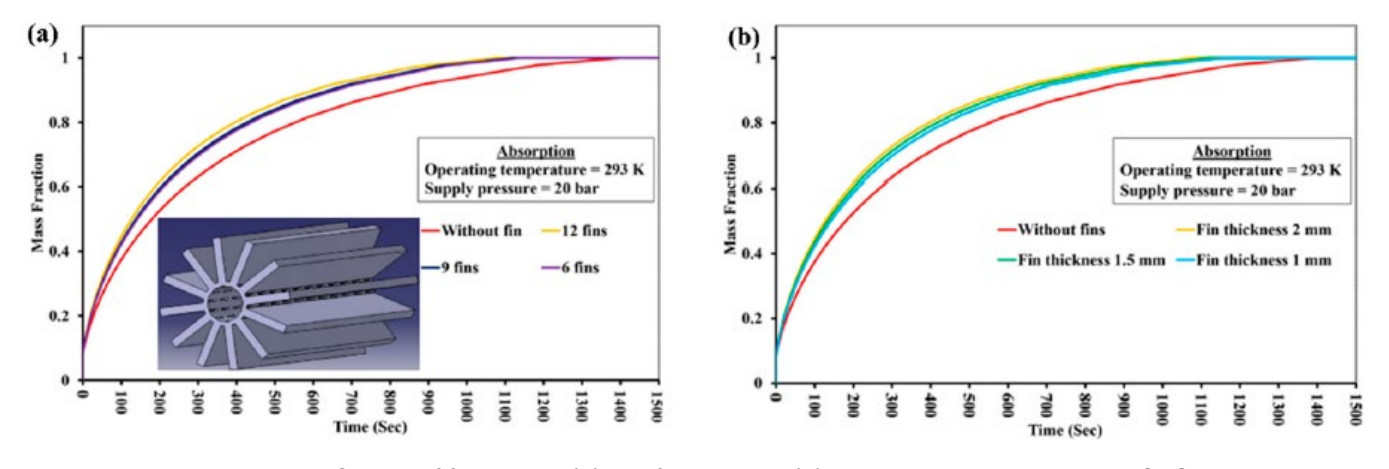


Figure 12 Influence of fin number (a) and fin thickness (b) on hydrogen absorption rate [49]

et al. evaluated a metal hydride reactor fitted with a finned tube heat exchanger. In the work of Gupta S. and Sharma V. K., copper internal longitudinal fins without complicated modification and an exterior water jacket were utilized. [32, 33].

Chapter 2 Bed reactor properties

2.1. Properties of the MH bed

2.1.1. Metal hydride basics

The reaction between a metal M and hydrogen may be represented as:

$$M + \frac{x}{2}H_2 \leftrightarrow MH_x \tag{1}$$

where x is the hydrogen-to-metal atomic ratio, usually written H/M. On a mass basis, the amount of hydrogen taken up is

$$w = \frac{xM_H}{M_M + xM_H} \tag{2}$$

where M_M is the average atomic weight of the metal atoms and M_H is the atomic weight of H. If the maximum amount of hydrogen taken up is $[H/M]_{max}$ in atomic terms or $[w]_{max}$

in mass terms, the reacted fraction is defined as

$$F = \frac{H/M}{[H/M]_{max}} = \frac{w}{[w]_{max}}$$
(3)

The absorption/desorption of hydrogen takes place in a range of pressures, between limiting concentrations that correspond to the phase boundaries of the pure dilute (α) and the pure concentrated hydride (β) phases. Ideally, according to the Gibbs Phase Rule the phase conversion occurs over a plateau at constant pressure in the pressure—composition isotherm, but real hydrides exhibit plateau slope and pressure hysteresis. Phase conversion has an associated enthalpy which is released/absorbed between the phase boundaries, while little heat is released/absorbed when changing the concentrations of the dilute and concentrated pure phases. [34]

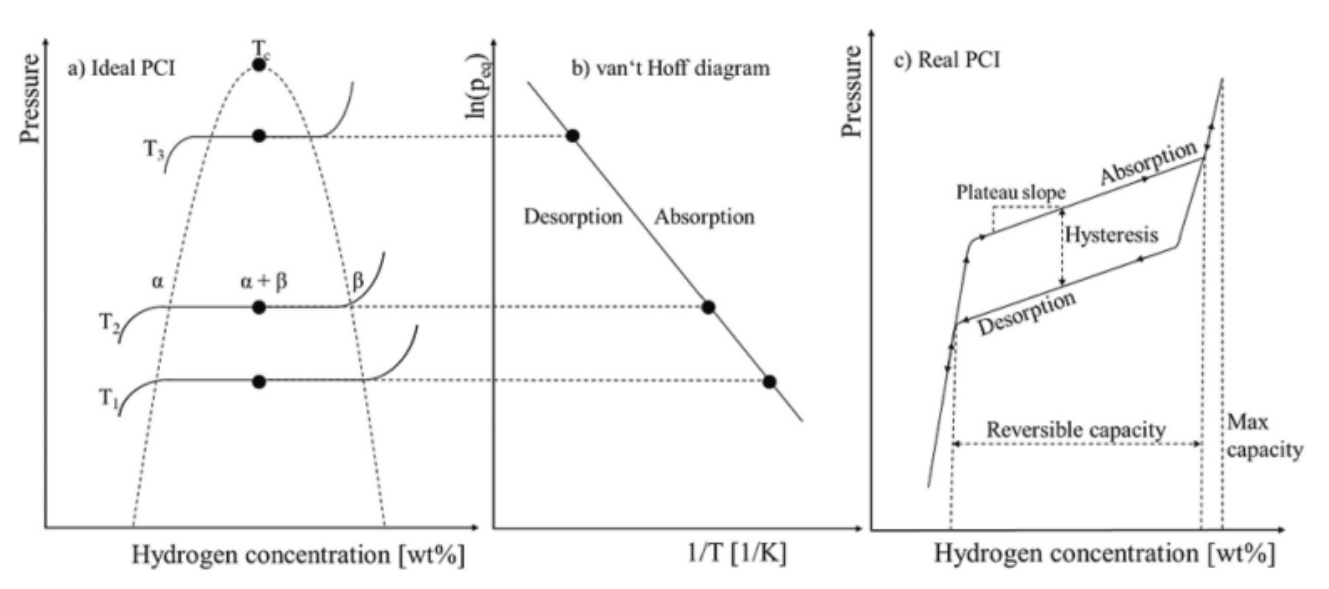


Figure 13 a) Ideal PCI at different temperatures with the corresponding b) van't Hoff plot and c) real PCI with hysteresis and plateau slope. [35]

2.2. The material choosing criteria

The manufacturing, activation, handling, and property improvements of a few chosen materials are covered in this section. Preference was given to materials with commercial or demonstration uses as well as those deemed most promising in the literature. Materials from various hydride groups are also chosen. The elemental hydrides group's most notable representative is Mg/MgH_2 . From the interstitial hydride group TiFe, $TiMn_2$ and $LaNi_5$ are chosen as representatives of the AB, AB2 and AB5 subgroups. One of the most heavily discussed complex metal hydrides is $NaAlH_4$ from the alanates group. Lastly, the complex borohydride $LiBH_4$ is selected due to it being the hydride material with the highest theoretical gravimetric capacity.

2.2.1. Magnesium hydride (MgH₂)

Magnesium hydride MgH_2 offers a high hydrogen storage capacity (~7.6 wt%) but suffers from slow kinetics, high desorption temperature (>400 °C), high enthalpy (~76 kJ/mol), and activation energy (~160 kJ/mol). Its surface easily oxidizes in air, requiring thermal or mechanical activation. Kinetics can be improved by doping with metals (Ni, Fe, Ti) or alloys, reducing desorption temperature and energy barriers. Carbon additives (graphene, CNTs) enhance cycling stability. Nanosizing (3–50 nm) increases surface area and diffusion, while nanoconfinement in porous scaffolds prevents particle agglomeration but reduces capacity. Synthesis methods include ball milling, CVD, melt spinning, and electrochemical deposition [35].

2.2.2. Titanium iron (TiFe)

TiFe is a well-known metal hydride alloy for hydrogen storage with a typical capacity of ~1.7 wt%, featuring two distinct pressure plateaus. Its main drawback is the need for activation, usually involving repeated cycling at 400–450 °C under ~65 bar H₂. It is sensitive to oxidation (forming TiO₂), which blocks hydrogen uptake, though partial recovery is possible through ball milling or cold rolling. TiFe is synthesized via arc melting, induction melting, or mechanical alloying; alternative methods like electrochemical reduction and gas atomization are under development. Alloying with Mn, V, or Co improves activation, lowers plateau pressures, and enhances cycling. Additives like Pd can also catalyze hydrogenation by surface modification. Substitution with elements like Mn, Al, Mg, or Si improves activation by reducing oxidation, while elements like Zr or Cr reduce capacity. DFT calculations guide alloy design, and combinations with other hydrides further enhance performance [36].

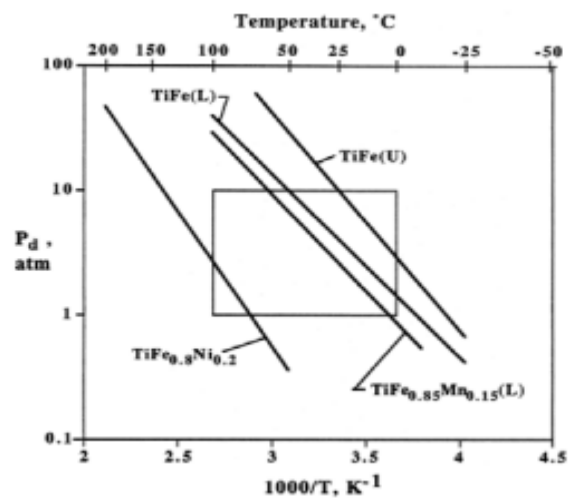


Figure 14 Van't Hoff's plots of alloys type AB [43]

2.2.3. Titanium Dimanganese (TiMn₂)

TiMn₂-based alloys are hydrogen storage materials known for their easy activation, good kinetics at room temperature, and relatively low cost. Typically synthesized by arc or induction melting followed by annealing (~1000 °C), they form non-stoichiometric Laves phases (TiMnx, x = 0.75–2), with TiMn_{1.5} offering the most stable plateau and best storage performance. They do not require thermal activation but must be protected from oxidation due to Mn's oxygen affinity. Their drawbacks include relatively high plateau pressure and significant hysteresis. These can be improved by partial substitution with elements like Zr, V, Cr, Ni, or Al. Zr reduces plateau pressure and enhances absorption capacity, though too much lowers reversibility. V offers the best pressure reduction and improved capacity, while excessive V or Al reduces plateau stability or capacity. Alloys like Hydralloy C5 (Ti-Zr-Mn-V-Fe) illustrate optimized compositions. Elemental substitution can also enhance kinetics significantly—up to 20–30× faster reaction rates compared to pure TiMn_{1.5}—demonstrating their high potential for tailored hydrogen storage applications [37].

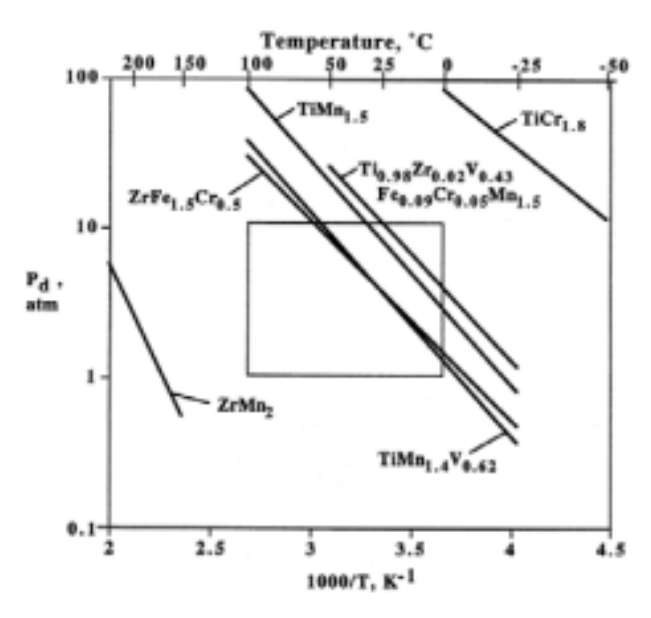


Figure 15 Van't Hoff's plots of alloys type AB2 [43]

2.2.4. lanthanum pentanickel (LaNi₅)

LaNi₅ is a widely used intermetallic hydride known for its easy activation, fast kinetics, and good resistance to air and impurities. It can be synthesized by arc, induction, or electron-beam melting, though alternatives like CaH₂ reduction of La₂O₃ and Ni offer more control. Activation occurs at mild conditions (<100 °C, <100 bar) without mechanical treatment. In fact, ball milling reduces storage capacity due to overly stable hydride formation at nanoscales, though annealing (~500–550 °C) can partially recover performance. LaNi₅ exhibits a flat pressure plateau (2–3 bar), with plateau pressure increasing slightly after processing. Handling is easier than for TiFe or TiMn₂ due to surface self-healing via Ni regeneration, but caution is required as LaNi₅ is flammable and toxic. Enhancements are achieved by partially substituting Ni with Al, Mn, or Co: Al significantly lowers plateau pressure, Mn maintains capacity while reducing pressure, and Co improves cycling life. Substituting La with Ce, Pr, or Nd can raise plateau pressure but improve cycling in certain cases (notably with Ce) [38].

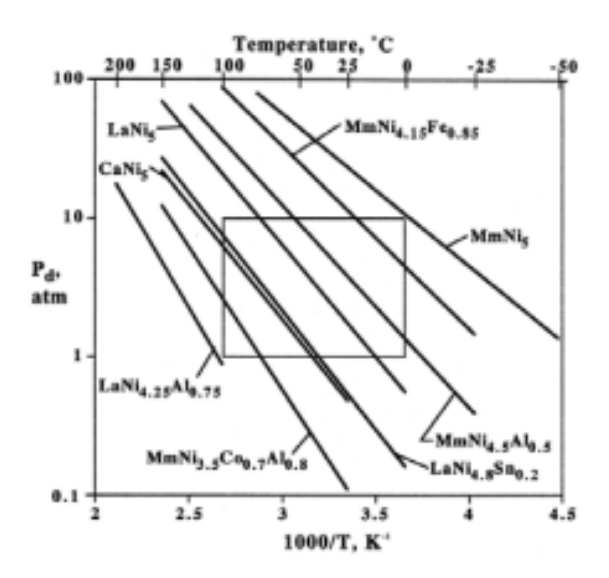


Figure 16 Van't Hoff's plots of alloys type AB5 [43]

2.2.5. sodium aluminum hydride (NaAl H_4)

NaAl H_4 is a complex hydride with a theoretical reversible hydrogen capacity of 5.5 wt% (practical ~5 wt%), releasing H_4 in two steps at ~30 °C and ~100 °C, followed by a non-reversible third step above 450 °C. It is typically synthesized by ball milling NaH and Al under H_4 at 130 °C and 90 bar, with alternative routes using recycled aluminum and catalysts like TiF₃. NaAl H_4 suffers from slow kinetics and poor reversibility, requiring high temperatures (200–400 °C) and pressures (100–400 bar) for rehydrogenation unless doped. Doping with TiCl₃ significantly improves reversibility at ~100 °C and 100 bar, while ScCl₃ enhances absorption rate further but introduces memory effects. CeCl₃ improves cyclic stability, though with reduced capacity. Other dopants include metal oxides, halides, carbon materials, and MOFs. NaAl H_4 must be handled under inert conditions due to high reactivity with moisture and its toxic, flammable nature [39].

2.2.6. lithium borohydride (LiB H_4)

LiB H_4 is a complex hydride with a high theoretical hydrogen capacity of 18.5 wt%, though only ~10 wt% is released below 680 °C. Its main drawbacks are slow kinetics, high desorption temperatures (\geq 400 °C), and harsh rehydrogenation conditions (\geq 600 °C, 70–350 bar). It can be synthesized via hydrogenation of Li and B, or through cation exchange between LiBr and NaB H_4 in solvents like THF. The material is highly reactive with moisture and poses fire hazards. To improve performance, methods include metal doping (e.g., Fe, Ti, Ni) to reduce desorption energy, partial substitution of Li⁺ or BH₄⁻ to destabilize the structure, and use of catalysts such as TiCl₃ or ZnF₂, which can lower desorption temperatures below 100 °C. However, reversibility remains limited. Nanostructuring through ball milling or nanoconfinement also enhances kinetics by increasing surface area, but full reversibility at mild conditions is still an open challenge [40].

2.3. Comparative criteria

In this review, key representatives from different categories of metal hydrides were analyzed for hydrogen storage applications: MgH₂ from elemental hydrides, TiFe, TiMn₂, and LaNis from interstitial hydrides, and NaAlH₄ and LiBH₄ from complex hydrides. MgH₂ stands out for its high hydrogen capacity (7.6 wt%) and abundance but operates only at high temperatures (>300 °C), limiting its practicality. Interstitial hydrides operate under mild temperatures and pressures, making them suitable for integration with existing hydrogen systems. Among them, TiFe and TiMn₂ are low-cost and effective but require activation and show hysteresis. LaNis, although more expensive due to rare-earth content, enables very easy activation and operates under the lowest pressure among the interstitial group. Complex hydrides such as NaAlH₄ and LiBH₄ provide high theoretical capacities, making them attractive for mobile uses, but suffer from slow kinetics, low reversibility, and require high temperatures and pressures, limiting their practical value.

Hydride	Advantages	Disadvantages
MgH ₂	 inexpensive and abundant high H₂ capacity (7.6 wt%) thermal stability good recyclability 	 sluggish kinetics and poor cycle stability very slow (first) hydrogenation high desorption temperature (300 °C, 1 bar) and enthalpy high sensitivity towards oxygen
TiFe	 inexpensive and abundant simple enhancement by substitution common good cycling stability at low pressure mild operating conditions 	 demanding conditions for (first) activation (400 °C under vacuum or H₂ atmosphere) relatively low gravimetric storage capacity low hydrogenation rate
TiMn ₂	(30–70 °C, 10–20 bar) • good recyclability • good kinetics • inexpensive and abundant • long-term stability/ durability • ambient operation	 high sensitivity towards gas impurities (CO/CO₂) and oxygen sensitivity towards gas impurities high equilibrium pressure plateau hysteresis effect "oxygen-affine"
LaNi ₅	temperature mild activation conditions low (ambient) operating temperature and pressure high hydrogenation rate	 low specific energy density, H₂ storage capacity (1.4 wt%) expensive
	 mild activation conditions high volumetric capacity good cycling stability high resistance towards gas impurities 	abundance: rare Earth material flammable
NaAlH ₄	 inexpensive and abundant relatively moderate operating temperature for complex hydride 	 slow hydrogenation kinetics and poor reversibility pyrophoric
LiBH ₄	light weight very high hydrogen storage capacity	 expensive and not abundant (Li) high desorption temperatures (> 300 °C) slow kinetics and rather poor reversibility

Table 3 Advantages and disadvantages of hydrides [47]

Chapter 2: Bed reactor properties

Given the focus of this work on solid-state hydrogen storage, LaNis emerges as the most suitable choice. It offers fast and easy activation, low operating temperatures and pressures, and good resistance to impurities, which reduces handling complexity and safety risks. Its stable hydrogenation behavior and compatibility with ambient operating conditions make it ideal for stationary or integrated storage systems. While cost remains a factor, its reliability and system compatibility make LaNis the most advantageous material for this application.

2.4. LaNi5 equations

2.4.1. Mass and energy conservation

Let the hydrogen mass flow rate into the system be $\dot{\varphi}$ per unit volume. For zero hydrogen flow, during absorption the local MH density ρ_s decreases, causing the local hydrogen gas density ρ_g to increase. The mass balance equations for the gas and solid are therefore. For hydrogen

$$\varepsilon \frac{\partial \rho_g}{\partial t} + \frac{1}{r} \frac{\partial (r \rho_g v)}{\partial r} = \dot{m} - \dot{\varphi} \tag{4}$$

and

$$(1-\varepsilon)\frac{\partial \rho_s}{\partial t} = \dot{m} \tag{5}$$

the hydrogen consumption during the hydrogenation, v is the superficial flow velocity of gas and ε is the porosity. Assuming ideal gas behavior, which is reasonable for the pressures typically encountered in MH tanks, the gas density is:

$$\rho_g = \frac{PM_{H_2}}{R_g T} \tag{6}$$

The mass source term \dot{m} can be written as

Absorption
$$\dot{m} = (1 - \varepsilon) (\rho_{sat} - \rho_s) \frac{\partial F}{\partial t}$$
 (7)

where ρ_s is the density of the solid phase (metal or hydride), ρ_{sat} is the density of the solid

phase when saturated with hydrogen, dF/dt is the rate of reaction. Eq. (6) assumes that the density of the MH particles changes linearly with reacted fraction, *i.e.* obeys Vegard's Law on average.

Assuming local thermal equilibrium, $T_g = T = T_s$ and a single common energy balance equation can be written:

$$(\rho C_p)_{eff} \frac{\partial T}{\partial t} = \frac{1}{r} \frac{\partial}{\partial r} \left(\mathbf{k}_{eff} r \frac{\partial T}{\partial r} \right) - \rho_g C_{pg} v \frac{\partial T}{\partial r} + \dot{m} \Delta H \tag{8}$$

here k_{eff} is the effective thermal conductivity of the MH bed, ΔH is the enthalpy of phase conversion, which is assumed to be constant, and $(\rho C_p)_{eff}$ is the effective thermal capacity of the MH bed, which can be expressed by a porosity-weighted function of the same quantities for the gas and MH as:

$$(\rho C_p)_{eff} = \varepsilon (\rho C_p)_g + (1 - \varepsilon)(\rho C_p)_s \tag{9}$$

2.4.2. Specific heat

The specific heat of the MH increases relative to that of the empty metal with the absorption of hydrogen. Nakagawa *et al.* [41] developed the following semi-empirical expression for LaNi5 which could be adjusted for other alloys:

$$(C_p)_s = \frac{6(3.1R + 10.4 \times [H/M]_{max}F)}{M_{Ms} + 6 \times [H/M]_{max}FM_H} \times 1000$$
 (10)

Here 3.1R is the assumed constant contribution to the molar specific heat from the metal and the contribution per added H mole of H is $10.4 \text{ J(mol. K)}{-1}$. The factor 6 is appropriate for $LaNi_5H_6$. The factor 1000 occurs because the atomic weights are in gram.

2.4.3. MH expansion

Metals expand reversibly when absorbing hydrogen. Vegard's Law is well obeyed by many simple metal hydrides within the pure dilute and concentrated phases and is assumed here as an average over many MH particles in the full range of reacted fraction. If the relative expansion is τ_p (approx. 0.24 for LaNi5), the density of the solid phase is then linearly related to the reacted fraction and can be expressed by [41]

$$\rho_S = \rho_{S,in} \frac{1 + F[w]_{max}}{1 + F\tau_p} \tag{11}$$

Where $\rho_{s,in}$ is the density of the empty metal alloys.

2.4.4. Effective thermal conductivity

For a uniform isotropic randomly packed assembly of perfect spheres with diameter D_p , Gusarov and Kovalev [42] obtained an exact expression for the effective thermal conductivity

$$k_{eff} = \frac{N(1-\varepsilon)}{\pi D_n R_c} \tag{12}$$

where N is the particle coordination number and R_c is the thermal contact resistance. The approach adopted here is based on this equation, with D_p taken to be the mean particle diameter of rough spheres and with a more realistic model of the actual contact between spheres. Expressions for the variables in Eq. (12) now need to be obtained in terms of the fundamental parameters introduced.

Assuming linear volume expansion,

$$D_p = D_{p,in} (1 + F\tau_p)^{1/3}$$
 (13)

Van de Lagemaat *et. al.* [43] found an empirical relationship between the effective coordination number of a random porous structure and its porosity as follows:

$$N = \frac{3.08}{\varepsilon} - 1.13\tag{14}$$

2.4.5. Rate of reaction

As mentioned, the apparent kinetics of hydrogen absorption/desorption by a MH bed is dominated by heat flow. The reason is that the intrinsic kinetics of the MH is typically fast compared to the real rate of change of the global hydrogen concentration, unless the MH is thermally clamped. This means that the MH is essentially in equilibrium with its surroundings at the local temperature and pressure. Supposing that the reaction is controlled by diffusion or the phase transformation, we may assume that the reaction is first-order or nearly so and therefore expect exponential time response. The other factors to be included are temperature dependence of the rate and the pressure drive, meaning the effect of the difference between the local hydrogen pressure and the equilibrium pressure corresponding to the local hydrogen concentration.

For absorption, with rate constant k_a

$$F = 1 - \exp\left(-k_a t\right) \tag{15}$$

and the reaction rate is

$$\frac{\mathrm{dF}}{\mathrm{dt}} = \mathrm{k_a} (1 - \mathrm{F}) \tag{16}$$

 $\frac{dF}{dt}=k_a(1-F)$ The pressure and temperature dependencies can be included in k_aas follows:

$$k_{a} = \frac{\kappa_{a}}{(1-\epsilon)} \exp\left(-\frac{E_{a}}{R_{g}T}\right) \ln\left(\frac{P}{P_{eq}^{a}}\right)$$
 (17)

Where κ_a is a material-dependent intrinsic absorption rate constant, E_a is a notional absorption activation energy capturing the temperature dependence of the rate, and Paq is the equilibrium absorption pressure.

2.4.6. **Porosity**

The average porosity of the MH bed is defined as

$$\varepsilon = 1 - \frac{V_s}{V_T} \tag{18}$$

where V_S is the total volume of solid particles and V_T is the total volume of the bed including particles and pores. The porosity varies owing to expansion of the individual MH particles during absorption and contraction during desorption by the relative factor au_p . The overall relative change in the total pore volume is not in general 1- τ_n , however, because of compaction caused by the increased mechanical pressure between the expanding particles, which offsets the increase in packing fraction [44].

calculated the resulting porosity relative to that of the empty MH bed, ε_0 , as follows

Absorption:

$$\varepsilon_a = 1 - (1 - \varepsilon_0) \left[\frac{1 + \tau_p F}{1 + \tau_a F} \right] \tag{19}$$

Where τ_a is the packed bed expansion ratio during absorption.

2.4.7. Gas velocity

For flow in the radial direction only, the superficial flow velocity, v, of the gas within the MH bed can be described by Darcy's law in the following form:

$$v = -\frac{K_P}{\mu} \frac{\partial P}{\partial r} \tag{20}$$

Where K_P is the permeability of MH bed and μ is the kinematic viscosity of the gas, taken to be constant in the relevant range of conditions. The permeability may be calculated using the Blake–Kozenye semi-empirical expression describing the laminar flow of a Newtonian fluid through a packed bed which is long and wide compared to the particle size [45]:

$$K_p = \frac{D_p^2 \varepsilon^3}{150(1-\varepsilon)^2} \tag{21}$$

The mean particle diameter may be obtained by direct measurement or in terms of a sphere equivalent relationship to the experimentally determined total surface area via the parameter a_v , defined as the ratio of the total particle surface area to the total volume of particles in the bed:

$$D_p = 6/a_v \tag{22}$$

Then Eq. (20) becomes

$$v = -\frac{D_p^2 \varepsilon^3}{150\mu(1-\varepsilon)^2} \frac{\partial P}{\partial r}$$
 (23)

2.4.8. Equilibrium pressure

The equilibrium (in the sense of quasi-static) absorption behavior of a metal hydride is generally captured by measuring pressure—composition isotherms in a range of temperatures. Absorption occurs when the local hydrogen pressure exceeds the equilibrium pressure, P_{eq} , at the local temperature. Very many equations have been proposed. The equation adopted here was developed by Mohammadshahi *et. al.* [46] for LaNis–H2, based on new experiments:

$$P_{eq} = \left[\frac{c_0 c_1 F^{c_2}}{1 + c_1 F^{c_2}} + c_3 F + e^{c_4 (F - c_5)} \right] \exp \left[-K \left(\frac{1}{T} - \frac{1}{T_{ref}} \right) \right]$$
(24)

Where $C_0 - C_5$ and K are fitted coefficients. The ideal value of K is $\Delta H/R$. The exponential builds-in the fact that most metal hydrides obey Arrhenius' Law. The leading terms account for the existence of a sloped plateau [46].

2.4.9. Heat transfer coefficient

In the case of forced convection of the circulating coolant through the heat exchanger, the average heat transfer coefficient for longitudinal flow over a cylinder can be found from the average Nusselt number as follows

$$h_f = \frac{\overline{Nu} \, k_f}{D_{tn}} \tag{25}$$

Chapter 2: Bed reactor properties

Where D_{tn} is the diameter of the tank and k_f is the thermal conductivity of the fluid. The average Nusselt number can be found from the following empirical relation presented by Bergman *et. al.* [45] as follows:

$$\overline{Nu} = 0.3 + \frac{0.62Re^{1/2}Pr^{1/3}}{[1 + (0.4/Pr)^{2/3}]^{1/4}} \left[1 + \left(\frac{Re}{282000}\right)^{5/8}\right]^{4/5}$$
 (26)

Where Re is the Reynolds number and Pr is the Prandtl number.

Chapter 3 Mathematical model and Numerical method

3.1. Simulation model

3.1.1. Model definition

illustrates the tank studied in this model. The tank is cylindrical and equipped with a water filled cooling jacket. The porous metal alloy is placed in cartridges that can be reached by the gas from a central distribution channel. The gas, in this case hydrogen with low amounts of nitrogen, enters the reactor from the top.

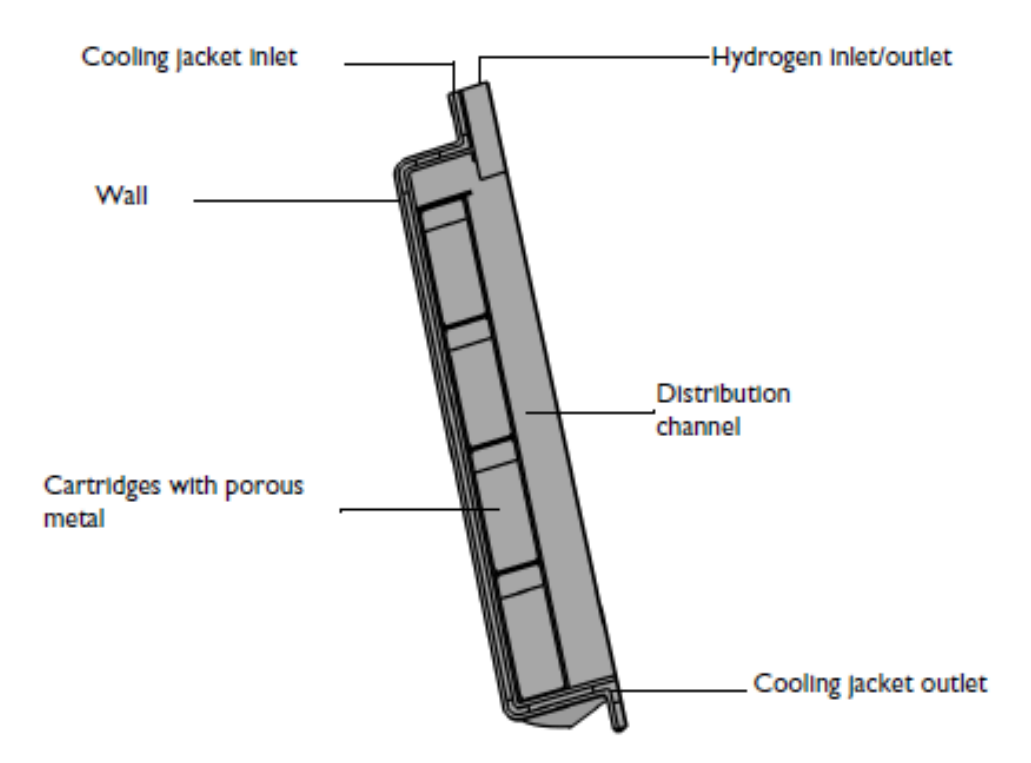


Figure 17 The studied model illustration

This is an academic model which is published by COMSOL Multiphysics, with a .pdf file which contain the steps to evaluate and apply the physics to a defined geometry to observe the adsorption process in a porous medium. Which can be realized.

Shows the modeled domain which consists of 1/8 of the tank geometry. This simplification can be made due to the geometric symmetry of the cartridges. To further simplify the geometry, and to save computational memory, the porous metal is modeled

as a porous medium.

The model is based on the following assumptions:

- The gas phase is modeled as an ideal gas
- The porosity and volume of the porous metal alloy does not change due to absorption
- Local thermal equilibrium exists in the porous bed
- Gravity effects are negligible

Chapter 3: Mathematical model and Numerical method



Figure 18 Illustration of 5/8 of the tank geometry without hydride alloy

The absorption rate of hydrogen atoms $\delta XH/\delta t$ (1/s) has been defined as [47, 48]

$$\frac{\partial}{\partial t}XH = C_a \exp\left(-\frac{E_a}{RT}\right) \ln\left(\frac{\rho_{H_2}}{p_{eq}}\right) (XH_{max} - XH) \tag{1}$$

where XH (mol/mol) is the number of absorbed hydrogen atoms per metal atom site

$$XH = \frac{n_H}{n_M} \tag{2}$$

 XH_{max} is the maximum number of hydrogen atoms that can be absorbed per metal site, C_a is a pre-exponential factor, E_a is the activation energy, ρ_{H_2} is the partial pressure of hydrogen, and p_{eq} is the equilibrium hydrogen pressure. The equilibrium pressure is related to the temperature as described by the van't Hoff equation. [49]

$$p_{eq} = (T, XH) = p_{iso}(T_{iso}, XH) \exp\left(\frac{\Delta H}{R} \left(\frac{1}{T} - \frac{1}{T_{iso}}\right)\right)$$
(3)

where ΔH (J/mol) is the entropy change due to absorption. The hydrogen pressure at isothermal conditions, p_{iso} , and the resulting absorbed hydrogen content (XH) comes from experimental data. [50]

Chapter 3: Mathematical model and Numerical method

The reaction rate of forming metal hydride R_{MH} (mol H /($m^3 \cdot s$)) can be expressed as a function of the absorption rate

$$R_{MH} = c_M \frac{\partial}{\partial t} XH \tag{4}$$

 c_M is the concentration of metal sites (M) in the solid phase that hydrogen atoms can react with (mol M/ m^3)

$$c_M = -\rho_S M_M \tag{5}$$

From stoichiometry, the reaction rate for H_2 (mol $H_2/(m^3.s)$) is

$$R_{H_2} = -\frac{R_{MH}}{2} \tag{6}$$

As hydrogen is absorbed and metal hydride is formed, heat (W/m^3) is released according to

$$Q_{abs} = -R_{MH}\Delta H \tag{7}$$

the maximum mass fraction of hydrogen atoms in the modeled alloy (M) is derived as following:

$$W_{H,max} = \frac{XH_{max}M_H}{M_M + XH_{max}M_H} = 0.0059$$
 (8)

Where M_i is the molar mass for species I and XH_{max} is 6 (mol H/mol M).

3.1.2. Fluid flow

The fluid flow of water in the cooling jacket is modeled as incompressible laminar flow. The inlet flow is assumed to be fully developed and an average inlet velocity is given. There is no slip at the jacket walls. The outlet has a pressure boundary condition with a static relative pressure equal to zero. There is no backflow at the outlet.

The fluid flow of hydrogen gas is modeled as a compressible, laminar flow, and described by the Navier-Stokes equations in the free flow parts, and the Brinkman equations in the porous material domain. The **Porous slip** formulation is used on boundaries adjacent to solid walls. This introduces slip velocity and relaxes the need for resolving the thin shear layer at the wall. A Darcian flow model is used in the porous domain. The inlet of the gas has a pressure boundary condition. Normal flow and no backflow is enforced.

The inlet pressure is gradually increased by 6 atm over 5 minutes. This improves the convergence rate of the system.

Symmetry boundary conditions are applied on each side of the modeled geometry.

3.1.3. Mass transfer

The incoming gas consists of mainly hydrogen. As absorption progresses, the hydrogen is removed from the gas, until mainly nitrogen remains. Since the gas phase consists of two species with comparative mole fractions, the system is described by the **Transport of Concentrated Species in Porous Media** interface. This interface solves for the mass transfer in the free flow domains and the porous domains. In the porous domains the conservation equations for hydrogen and nitrogen are:

$$\varepsilon_{p}\rho \frac{\partial \omega_{H2}}{\partial t} + \nabla j_{i} + \rho(u.\nabla)\omega_{H2} = (\varepsilon_{p} - \omega_{H2})Q_{mass}$$

$$\varepsilon_{p}\rho \frac{\partial \omega_{N2}}{\partial t} + \nabla j_{i} + \rho(u.\nabla)\omega_{N2} = -\omega_{H2}Q_{mass}$$
(9)

where ε_p is the porosity, ω_i is the mass fraction of species I, j_i is the mass flux (kg/m^3) , **u** is the velocity vector (m/s), and Q_{mass} is the mass source $(kg/(m^3 \cdot s))$ due to absorption. The terms in the mass conservation equations for the free flow domains are the same as for the porous domain except that the porosity is one and there are no mass sources.

The mass flux the system consists of convective and diffusive flux. The diffusive flux is described with the **Mixture-averaged** diffusion model. This model is a simplification of the Maxwell-Stefan model, and it is suitable when the multicomponent diffusion can be assumed to be constant as a function of partial pressure and temperature. In the porous domain the diffusivity is affected by the porosity. The resulting effective diffusivity is described by the **Bruggeman model**.

As mentioned, the reaction source is only defined in the porous domain. The mass source (kg $H_2/(m^3 \cdot s)$) of hydrogen gas being absorbed into the solid matrix is:

$$Q_{mass} = \varepsilon M_{H2} R_{H2} \tag{10}$$

where ε is the porosity of the alloy. This mass source is automatically added as a mass source to the fluid flow interface by the **Reacting Flow** Multiphysics coupling.

The gas inflow has a given mole fraction as the boundary condition. As for the fluid flow description, symmetry boundaries for the mass transfer are used to reduce the modeling domain.

3.1.4. Heat transfer

Heat transfer through convection and conduction is modeled by the **Heat Transfer In Porous Media** interface. In the porous domains, **Local thermal equilibrium** is assumed, which means that the temperatures of the solid and the fluid are assumed to be the same. The energy balance for the system is

$$(\rho C_p)_{eff} \frac{\partial T}{\partial t} + \rho_f C_{pf} u \cdot \nabla T = \nabla \cdot \left(k_{eff} \nabla T \right) + Q_{abs}$$
(11)

where ρ_f (kg/ m^3) is the fluid density, C_{pf} (J/(kg·K)) is the fluid heat capacity, $(\rho C_p)_{eff}$ (J/(m^3 ·K)) is the effective volumetric heat capacity, and k_{eff} (W/(m·K)) is the effective thermal conductivity. Furthermore, u (m/s) is the fluid velocity field, derived by the fluid flow interface. Q_{abs} (W/ m^3) is the heat released as hydrogen is absorbed into the solid alloy and reacts to form metal hydride. This heat source is automatically added to the heat transfer interface by the Reacting Flow Multiphysics coupling.

Chapter 3: Mathematical model and Numerical method

The effective conductivity of the solid-fluid system, k_{eff} , is related to the conductivity of the solid, k_s and to the conductivity of the fluid, k_f , by

$$k_{eff} = \theta_s k_s + \theta_f k_f \tag{12}$$

Here θ_s denotes the solid material's volume fraction, which is related to the volume fraction of the fluid θ_f (or porosity) by

$$\theta_s + \theta_f = 1 \tag{13}$$

The heat transfer interface in the gas and porous media domains. For the solid alloy in the tank, only heat transfer by conduction applies:

$$-\nabla . (k_s \nabla T) = 0 \tag{14}$$

where k_s (SI unit: W/(m·K)) is the thermal conductivity of the solid.

To increase the absorption rate, the reactor is cooled by a water filled cooling jacket. **Inflow** and **Outflow** boundary conditions define this flow. The initial temperature in the tank is 15°C, while the inflow temperature in the cooling jacket is 5.5°C.

3.2. Chosen characteristics

In the following section, we present the selected characteristics of the hydrogen storage tank. These parameters were chosen based on technical requirements, literature data, and compatibility with the metal hydride material $LaNi_5$. The geometrical dimensions, material properties, and thermal boundary conditions are detailed to provide a clear basis for the numerical modeling and thermal performance analysis.

Name	Symbol	Value/ Expression	
Thickness, cartridge	tCart	2 mm	
Height, cartridge	hCartSection	85 mm	
Radius, Reactor	rReac	rInnerCart+dMH+2*dCart=0.064 m	
Wall thickness, Reactor	tReac	3 mm	
Radius, Inner position of cartridge	rInnerCart	30 mm	
Thickness, metal hydride	tMH	30 mm	
Height, metal hydride	hMH	hCartSection*0.8= 0.068 m	
Radius, inlet pipe	rInlet	20 mm	
Outer height, Reactor	hReactor	2*tReac+cartNum*hCartSection+0.3*hCartSection= 0.3715 m	
Thickness, inlet pipe	tInlet	2 mm	
Radius, cartridge holes	rCartHole	7 mm	
Top height, inlet pipe	hTopInlet	hReactor*0.12=0.04458 m	
Inner height, inlet pipe	hInnerInlet	7 mm	
Height, cooling pipe, outlet	hOutletCoolingPipe	3 cm	
Radius cooling pipe, outlet	rOutletCoolingPipe	0.5 cm	
Thickness, cooling channel	tCoolingChannel	4 mm	
Thickness, Reactor outer wall	tReactorOuterWall	3 mm	
Number of cartridges	cartNum	4	

Table 4 The model's geometry parameters

3.2.1. Geometry selection

The table below presents the main geometrical parameters of the metal hydride tank. It includes all relevant dimensions such as cartridge size, tank thickness, pipe radii, and the configuration of the cooling channels and cartridges. These parameters define the structural layout used in the simulation and design of the storage system.

3.2.2. Input parameters

The table below presents the essential input parameters used for the numerical simulation of the hydrogen absorption process. These include physical, thermal, and operating conditions required to define the behavior of the system and ensure accurate representation in the computational model.

Name	Symbol	Value/Expression
Initial ratio of absorbed hydrogen atoms per metal atom	XH0	0.5
Maximum number of hydrogen atoms per metal atom	XHmax	6
Inlet temperature for cooling media	ТО	15 [degC]
Hydrogen molar mass	M_H2	2.01596 [g/mol]
Initial mean molar mass	M0	x0*M_H2+= 3.316 g/mol
Initial H2 mass fraction, gas phase	w0_H2	(x0*M_H2)/M0= 0.578
Initial pressure	P0_eq	x0/(1-x0)*P0= 1.93e6 Pa
Initial H2 mass, gas phase	m0_H2	rho0*V0*w0_H2= 81 g
Initial density	rho0	P0*M0/(R_const*T0)= 140.24 g/m^3
Alloy porosity	porMH	0.5
Alloy molar mass	MnM	421.5 [g/mol]
Heat capacity, alloy	СрМ	445 [J/g/K]
Alloy solid phase density	rhoM	7266 [kg/m^3]
Alloy heat capacity at constant pressure	СрМН	445 [J/g/K]
Hydrogen gas heat capacity	СрН2	28.7 [J/mol/K]
Hydrogen gas thermal conductivity	kH2	2.18 [W/m/K]

Chapter 3: Mathematical model and Numerical method

Dynamic viscosity for gas mixture	visc	1e-5 [Pa.s]
Inlet pressure	Pin	7 [atm]
Heat transfer coefficient	htc	2000 [W/m^2/K]
Temperature, cooling water	Tcooling	5.5 [degC]
Flow rate, cooling water	Fcooling	0.4 [m^3/h]
Area inlet pipe, cooling water	Ain	pi*((rInlet+tCoolingChannel)^2- rInlet^2)=5.5292e-4 m^2
Inlet velocity, cooling water	Vcooling	Fcooling/Ain= 0.20095 m/s
Number of geometry sectors	sectorNum	8

Table 5 Input parameters of the simulation model

This table presents the kinetic parameters governing the hydrogen absorption reaction in the metal hydride. These values are essential for describing the reaction rate, characterizing the energy barrier, and defining the thermodynamic behavior of the system during the absorption process.

Name	Symbol	Value
Enthalpy change due to absorption	deltaH	-29e3 [J/mol]
Activation energy	Ea	21.17e3 [J/mol]
Pre-exponential factor	Ca	59.187 [1/s]

Table 6 The models kinetic parameters

The kinetic and thermodynamic parameters of the alloy and hydrogen are taken from the following references [51, 52, 53].

3.3. COMSOL Multiphysics interface

3.3.1. Meshing

The following picture presents the conducted mesh, including corner refinement, types of mesh in each domain and the boundary layers.

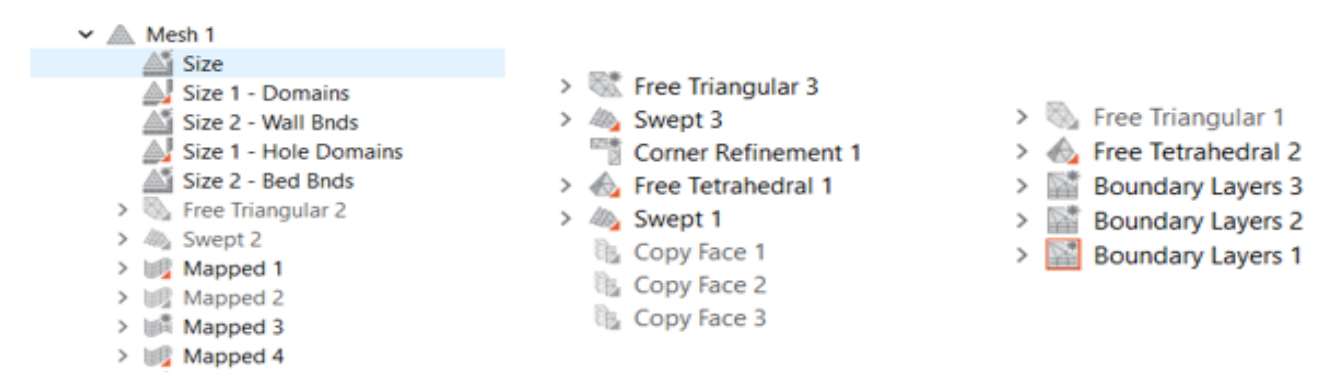


Figure 19 Illustration of the meshs conducted

Build Selected Build All Label: Size **Element Size** Calibrate for: General physics 200 Predefined mm Custom **Element Size Parameters** Maximum element size: 28.24 mm Minimum element size: 0.9 mm Maximum element growth rate: 1.45 100 Curvature factor: 0.5 Resolution of narrow regions:

The following figure shows an example of a mesh conducted

Figure 20 Meshing example interface

3.3.2. Physics used in simulating absorption

0.6

The simulation model incorporates multiple physics interfaces to accurately represent the coupled phenomena occurring during hydrogen absorption in the metal hydride tank.

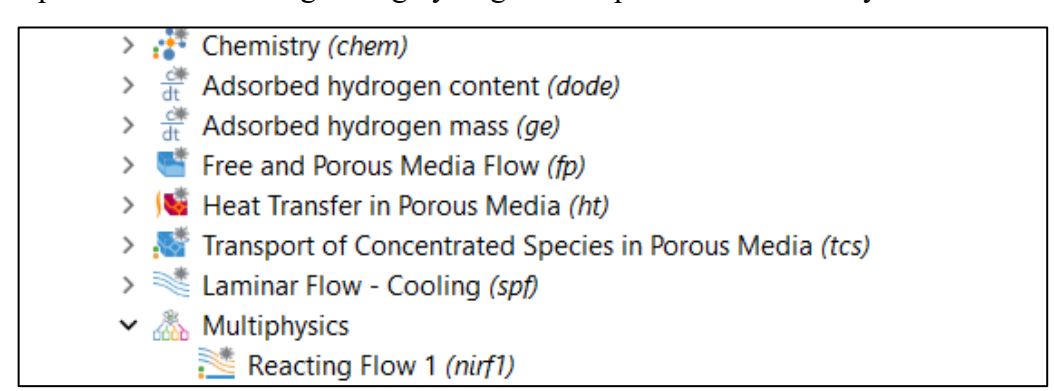


Figure 21 The physics used interface

- The Chemistry interface is used to define the reaction kinetics and track the absorbed hydrogen content over time.
- ♣ The Free and Porous Media Flow interface handles gas transport by coupling flow dynamics with the porous structure of the hydride.

Chapter 3: Mathematical model and Numerical method

- Heat Transfer in Porous Media captures the thermal effects caused by the exothermic absorption reaction and conduction within the porous material.
- ♣ The Transport of Concentrated Species in Porous Media is applied to model multicomponent gas transport with varying concentrations, and it governs the diffusion and accumulation of hydrogen within the solid bed. While Laminar Flow (Cooling) governs the liquid cooling circuit that ensures thermal regulation of the system.

Together, these interfaces allow for a fully coupled Thermos-chemical-fluid simulation, ensuring a realistic prediction of system performance.

3.3.3. Studies conducted

Two separate studies were carried out to simulate the hydrogen storage process in the metal hydride tank. The first study is a stationary analysis focused on the cooling water flow, aiming to determine the steady-state distribution of temperature and velocity within the cooling circuit. This step ensures that appropriate thermal boundary conditions are established before the absorption process begins. The second study is a time-dependent analysis that simulates the hydrogen absorption process over time. It captures the transient evolution of temperature, pressure, and hydrogen concentration in the metal hydride bed, allowing for an accurate assessment of the dynamic behavior of the system during charging.

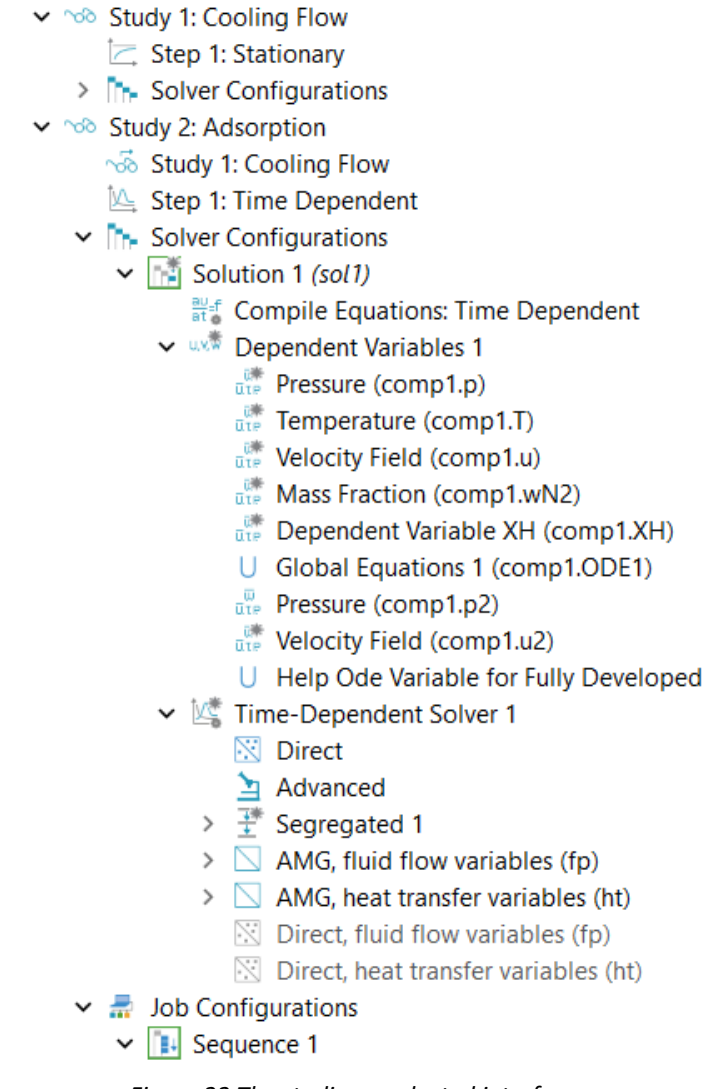


Figure 22 The studies conducted interface

3.4. Time dependent solver

An implicit BDF (Backward Differentiation Formula) scheme was employed to ensure numerical stability and efficient convergence for the stiff coupled equations of heat and mass transfer within the metal hydride reactor.

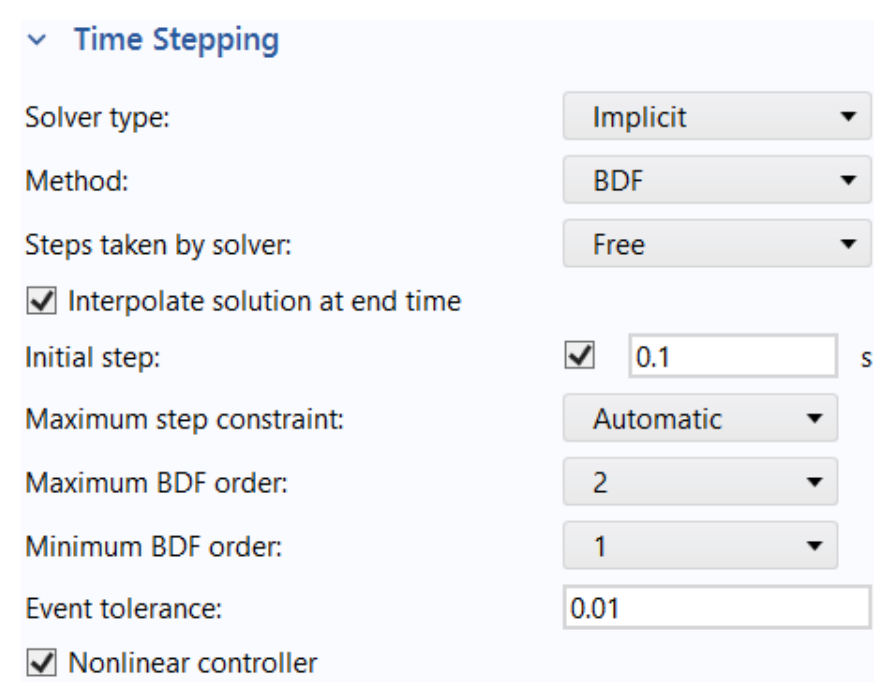


Figure 23 Illsutration of the solver interface

3.5. Materials definition

The materials and their defined parameters in COMSOL are available in the COMSOL material library, and their properties (such as heat capacity, density, and thermal conductivity) can be modified according to the specific requirements of the simulation.

in this window after choosing the materials, we have selected the domain of each one.

Materials	Type
Intermetallic alloy	Metal hydride, <i>LaNi</i> ₅
Structural steel	AISI 304 Stainless Steel
Cooling fluid	Water
Gas	Hydrogen H ₂

Figure 24 Table of the materials used in the simulation

Chapter 4 Results and discussions

4.1. Results obtained from simulation

4.1.1. Mesh dependency

To ensure the reliability of the simulation results, a mesh sensitivity analysis was conducted. Several mesh sizes were tested and compared based on their impact on the hydrogen absorption behavior. The key factor used to evaluate mesh quality was the evolution of the absorbed hydrogen quantity over time. The results showed that as the mesh was refined, the absorption curves progressively stabilized, indicating numerical convergence.

The final mesh was selected as a compromise between accuracy and computational efficiency, it provided consistent and reliable results without excessively increasing the simulation time.

Meshing	Domain elements	Absorbed H ₂ (g)	CPU time
Min (up to 3 mm)	Can't evaluate	No result	Not conducted
Min (2mm)	2060033	22.637298	1d 3hr
Min (1mm)	2068295	22.638136	1d 8hr
Min (0.9 mm)	2072766	22.368706	1d 11hr

Table 7 Table showing the meshing conducted with CPU time and absorbed mass of H2

Relative error

$$\Delta m_{H2} = \frac{22.637298 - 22.368706}{22.368706} = 0.012 = 1.2\%$$

The relative error is under 3%, we conclude that this allows us to choose the less dense mesh.

- ♣ Due to the limited computational capacity of the available PC, the simulation required a relatively long time to reach the final stabilization. This is mainly attributed to the weak processing power and RAM, which slowed down the calculation speed despite the simplicity of the model setup.
- The meshing refinement was limited to a minimum element size of approximately 3 mm because certain geometrical sections, such as the wall thickness, have dimensions around this value. Reducing the mesh size below 2 mm would not provide meaningful additional accuracy within these thin regions and could cause unnecessary computational load without improving the solution convergence or quality. That is the reason we've chosen 2mm as final mesh choose.

4.1.2. Absorbed hydrogen content

The following figure illustrates the distribution of absorbed hydrogen content and temperature within the metal hydride bed during the charging process. The hydrogen content map shows how the alloy stores hydrogen over time through absorption, while the temperature distribution reveals the heat generated by the exothermic reaction and its propagation throughout the bed. This combined visualization helps assess both storage efficiency and thermal behavior during the absorption phase.

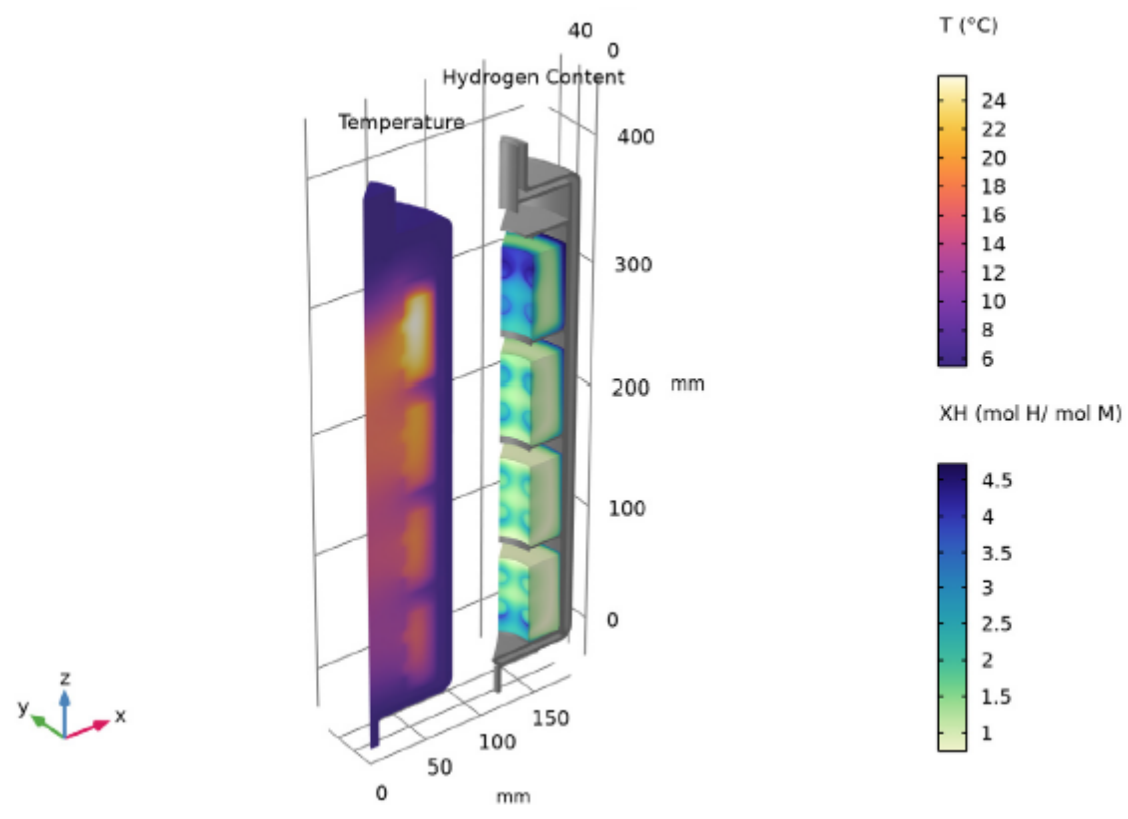


Figure 25 Hydrogen content and temperature distribution

4.1.3. Hydrogen mass profile

The following plot illustrates the evolution of hydrogen mass within the system over time. It includes the cumulative integral of hydrogen influx, representing the total mass of hydrogen introduced into the tank; the cumulative integral of absorbed hydrogen, indicating the amount chemically stored in the metal hydride; and the change in hydrogen mass in the gas phase, showing the remaining hydrogen in the void spaces. All quantities are expressed in grams. This comprehensive view allows for tracking mass conservation and assessing the efficiency of the absorption process.

Chapter 4: Results and discussions

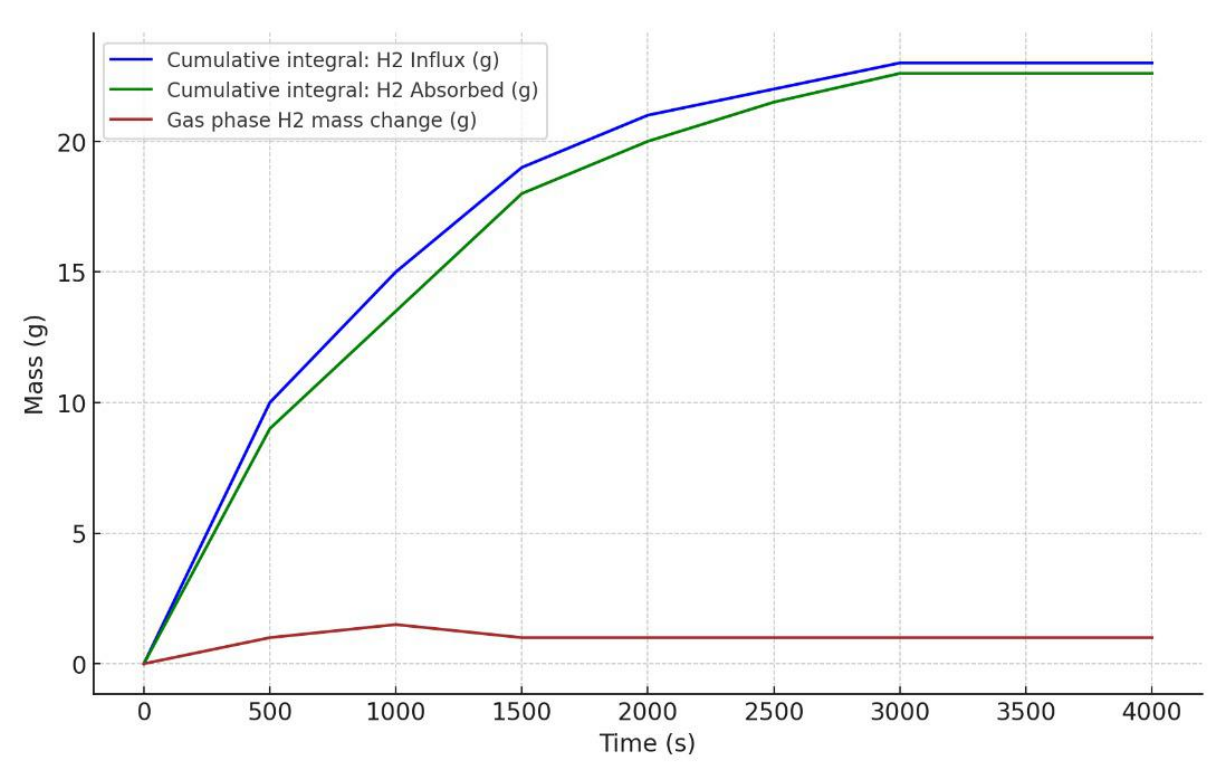


Figure 26 Plots of the hydrogen influx, adsorbed and mass change

The stabilization of the plots indicates that the system has reached saturation.

4.1.4. Evolution of Hydrogen content over time

The following plot shows the evolution over time of three key variables during the hydrogen charging process: the gas phase temperature, the bed temperature, and the charged hydrogen content (XH). The temperature curves reflect the thermal response of both the gas and solid phases due to heat generation from the absorption reaction.

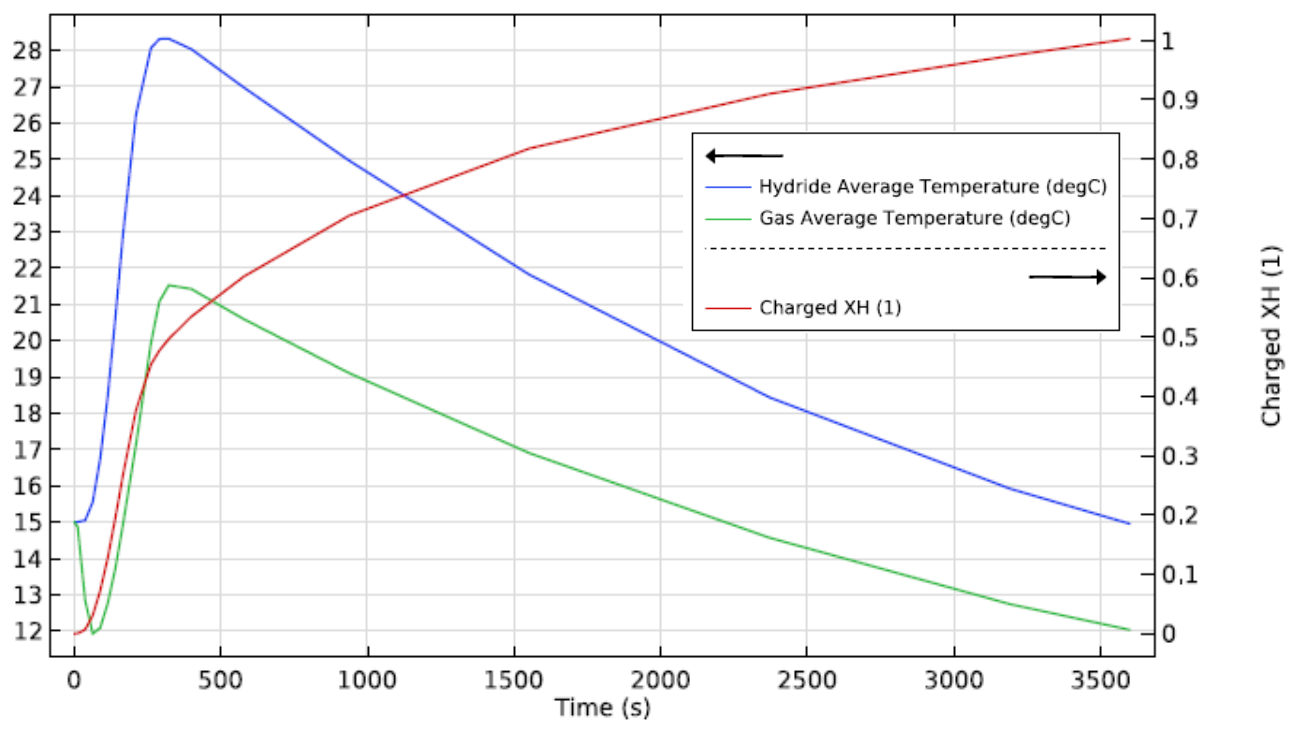


Figure 27 Plots of XH, Hydride and Gas temperature

Chapter 4: Results and discussions

The XH curve represents the progression of hydrogen uptake by the metal alloy. Together, these curves provide insight into the thermal and reactive dynamics of the system throughout the absorption process.

4.1.5. Pressure Evolution

The following plot displays the evolution of pressure and temperature within the metal hydride tank during the absorption process. The pressure curve reflects the gas dynamics and its interaction with the solid phase, while the temperature curve captures the thermal response driven by the exothermic nature of hydrogen absorption. Monitoring both variables over time is essential to understanding the system's behavior and ensuring optimal operating conditions.

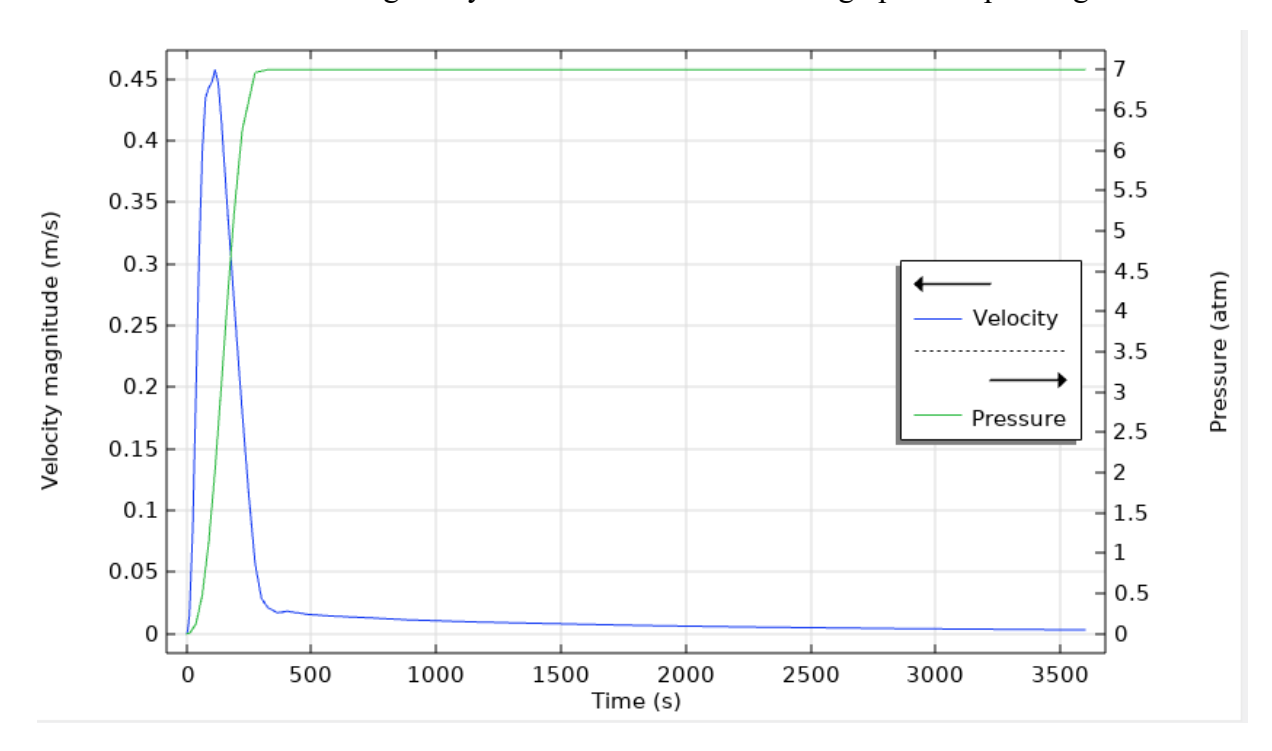


Figure 28 Pressure and Temperature evolution over time

4.2. Investigation of the simulation results validity

4.2.1. Comparative analysis with experimental results

To validate the accuracy of our model, the simulation results will be compared with available experimental data. This comparison will focus on key variables such as hydrogen absorption behavior, temperature evolution, and pressure trends. Matching these results provides confidence in the predictive capability of the simulation and ensures that the physical phenomena have been properly captured.

♣ Simulation

The following table presents key results obtained from the simulation, including the metal hydride volume, hydride density, total hydride mass, and the mass of hydrogen absorbed during the process. It also includes the weight fraction of stored hydrogen, the coolant temperature, and the simulation time setup. These values provide a summary of the system's performance under the given operating conditions.

Parameter	Value
Metal Hydride Volume V_{MH}	299,610 mm³ (0.2996 L)
Hydride Density ρ_{MH}	8300 kg/m^3
Hydride Mass m_{MH}	2.49 kg
Absorbed Hydrogen Mass m_{H2}	22.63 g
Weight Fraction of Hydrogen wt	0.0091 (0.91%)
Coolant Temperature	5.5 °C
Absorption time	3000 seconds

Table 8 Key results obtained from simulation

Experimental Study Summary (Souahlia et al., 2014)

The experimental study by Souahlia et al. (Experimental study of metal hydride-based hydrogen storage tank at constant supply pressure 2014) investigated a real hydrogen storage tank using LaNi5 metal hydride.

The experiment involved constant hydrogen supply pressure and a spiral-coil heat exchanger for improved heat transfer.

Chapter 4: Results and discussions

Parameter	Value
Hydride Mass m_{MH}	1.0 kg
Hydrogen Absorbed m_{H2}	11.0 g
Weight Fraction of Hydrogen XH	0.011 (1.1%)
Hydrogen Supply Pressure	20 bar
Coolant Temperature	15 °C
Absorption Time	2000 seconds

Table 9 Key results obtained from the experimental study

Calculations and quantitative comparison

Simulation:

$$XH_{sim} = \frac{m_{H2}}{m_{MH}} = \frac{22.63}{2490} = 0.0091$$

Experiment:

$$XH_{exp} = \frac{m_{H2}}{m_{MH}} = \frac{11}{1000} = 0.0011$$

Relative difference in weight fraction:

$$\Delta XH = \frac{XH_{exp} - XH_{sim}}{XH_{exp}} \times 100 = \frac{0.011 - 0.0091}{0.011} \times 100 = 17.27 \%$$

The COMSOL simulation results show a good physical correlation with experimental findings from Souahlia et al. The absorbed hydrogen quantity and weight fraction are proportionally consistent considering the larger MH mass and different boundary conditions. The slight underperformance in hydrogen fraction and the longer absorption time in simulation can be attributed to the lower coolant temperature and possibly lower hydrogen, pressure.

This indicates that the COMSOL model is physically valid and reliable for predicting hydrogen absorption behavior in LaNi5-based tanks.

4.2.2. Investigation of mesh dependency

Although the original study did not report a mesh dependency analysis, such an investigation was essential to ensure the reliability of the numerical results. A mesh sensitivity study was therefore performed using a 3D model of the cylindrical hydrogen storage tank containing 1 kg of metal hydride material. Two different mesh densities were applied: a coarse mesh and a fine mesh comparing to the established one. The comparison between the three configurations showed that the difference in absorbed hydrogen remained under 7%, confirming the mesh independence of the solution. This result validates the numerical stability and accuracy of the developed model.

Meshing	Domain elements	Absorbed H ₂ (g)	Relative error
Coarse	18525	10.87701	2.294 %
Published	52000	11.13244	
Fin	93120	11.89812	6.877%

Table 10 Mesh dependency of the published model

4.3. Sizing study

As part of the validation of a COMSOL Multiphysics model, an analysis was conducted to study the quantitative relationship between the mass of MH and the amount of hydrogen stored, using three simulated cases and extrapolation.

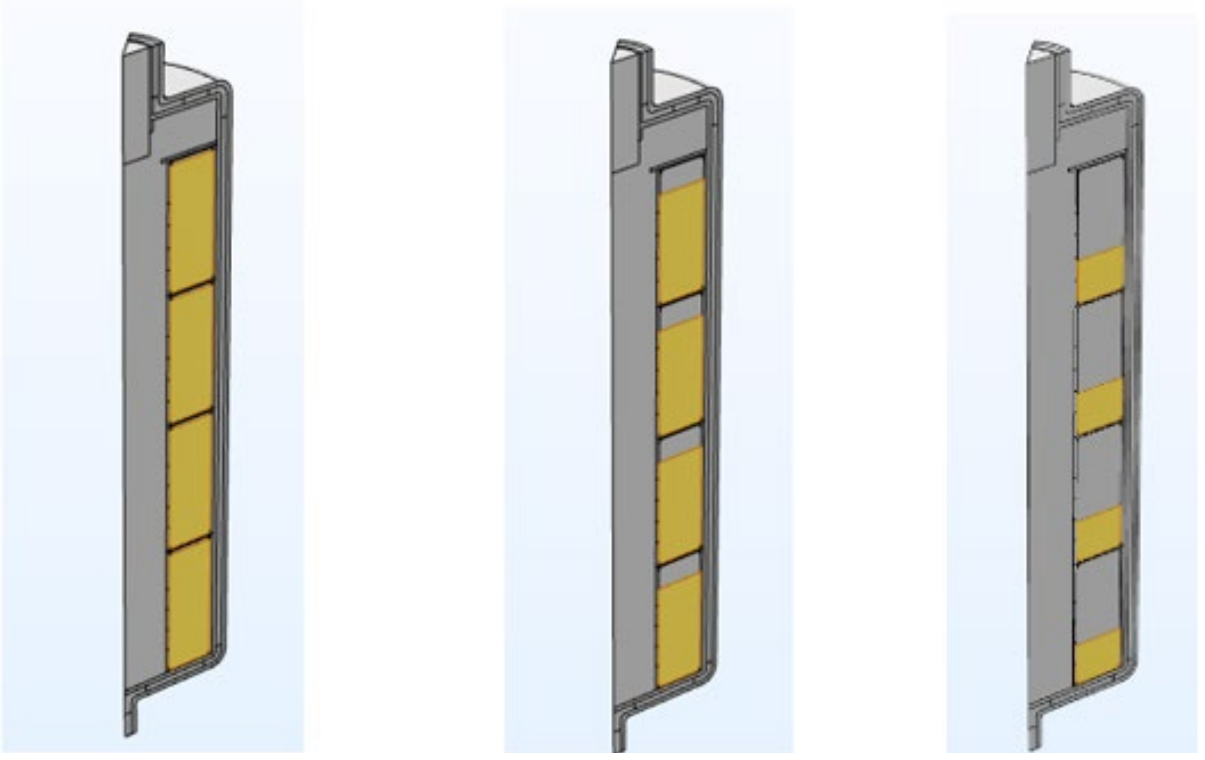


Figure 29 The studied models with different alloy mass

To study the influence of the alloy quantity on hydrogen storage performance, the same simulation procedure was repeated with a higher volume of metal hydride. In the first case, the hydride height was set to 0.8 times the cartridge section height, while in the second case it was increased to 0.95 times, and the third one is aimed to obtain 1kg of metal hydride alloy to compare it with an experimental study with the same amount of alloy. This variation allowed us to assess the effect of hydride sizing on the absorbed hydrogen content and to examine the proportional relationship between alloy volume and storage capacity.

♣ All the parameters are kept including geometry, we have varied just the mass of the alloy including its height.

4.3.1. Simulation Data from COMSOL

Three cases of simulations with different masses of metal alloy were carried out to confirm the proportionality between the metal hydride mass and the amount of absorbed hydrogen.

Case	MH Bed Height	MH mass	Absorbed H ₂ Mass (g)
First case	68 mm	2.49 kg	22.63 g
Second case	80.75 mm	2.95 kg	27.13 g
Third case	27.2 mm	1 kg	9.82 g

Table 11 Simulations obtained data

Ratio analysis

By analyzing the ratio of hydride heights and the corresponding absorbed hydrogen masses, we aimed to evaluate whether the increase in storage capacity follows a linear trend. The following calculations illustrate this comparison.

The approximates values using proportionality are depending on the result of the real experimental case of Souahlia (1kg of MH \rightarrow 11 g of H_2):

$$\sim m_{H2,1} = 27.39 \ g$$
 $\sim m_{H2,2} = 32.45 \ g$ $\sim m_{H2,3} = 11 \ g$

Chapter 4: Results and discussions

Relative error

$$\Delta m_1 = \frac{27.39 - 22.63}{22.63} = 0.2103 = 21.03 \%$$

$$\Delta m_2 = \frac{32.45 - 27.13}{27.13} = 0.196 = 19.6 \%$$

$$\Delta m_3 = \frac{11 - 9.82}{9.82} = 0.1202 = 12.02 \%$$

$$\Delta E = \frac{21.03 + 19.6 + 12.02}{3} = 17.54\%$$

The plots show an exponential curve, and the errors are above 15%. Therefore, we conclude that the relationship between the metal hydride mass and the absorbed hydrogen is not proportional. We cannot apply a simple rule of three, and a proper correlation must be established.

Comment

Recent literature (Hilali, 2016; Zhuo et al., 2021) indicates that under constant thermodynamic conditions (temperature and pressure) and for a given material, the amount of hydrogen stored is approximately proportional to the MH mass.

General conclusion

General conclusion

This work has laid the foundation for the digital prototyping of a solid-state hydrogen storage system based on metal hydrides. Through the development of a detailed 3D numerical model using COMSOL Multiphysics, we have simulated the hydrogen absorption process inside a cylindrical hydride tank under realistic thermal and geometric conditions. The project focused exclusively on the absorption phase, incorporating a full set of validated equations for kinetics, thermodynamics, heat transfer, and gas flow in porous media.

Understanding the absorption mechanism was essential to properly dimension the system and evaluate its performance. The role of geometry, was studied to investigate its influence on storage capacity. Simulations were conducted with varying hydride volumes to assess proportionality between alloy quantity and hydrogen uptake, showing strong linearity and consistency.

The mesh sensitivity analysis ensured that the spatial discretization did not distort the results, allowing us to identify a configuration that balances accuracy and computational time.

In addition, cooling through a stationary fluid study was performed to determine the initial thermal state before absorption. This made it possible to couple the heat transfer phenomena with the absorption kinetics in a more physically consistent manner.

The modeling framework developed here is general enough to be reused or extended for future optimization studies, including the integration of improved heat exchangers or more complex alloy structures. Moreover, the comparison between simulation outputs and experimental data provides confidence in the model's predictive capability.

We hope this work will provide future researchers and engineers with a structured and validated approach to designing and analyzing hydrogen storage systems based on metal hydrides. Future directions may include:

- 1. Experimental validation using real tank prototypes.
- 2. Full-cycle simulation covering both absorption and desorption.
- 3. Integration with a fuel cell or thermal system to evaluate performance in application-specific environments.
- 4. Investigation of advanced geometries or embedded cooling structures to improve heat management.

This thesis contributes to the growing efforts to develop clean and efficient hydrogen technologies and brings us one step closer to practical, compact, and safe hydrogen storage solutions.

- [1] "Lee, S.Y.; Lee, J.H.; Kim, Y.H.; Kim, J.W.; Lee, K.J.; Park, S.J. Recent Progress Using Solid-State Materials for Hydrogen Storage: A Short Review. Processes 2022, 10, 304," 2022.
- [2] International Energy Agency (IEA). The Future of Hydrogen: Seizing Today's Opportunities. Report prepared by the IEA for the G20, Japan, 2019..
- [3] Goebel, E., Coveney, Jr., R.M., Angino, E.E., Zeller, E.J., and Dreschoff, G.A.M., Geology, composition, isotopes of naturally occurring H2/N2 rich gas from wells near Junction City, Kansas, Oil Gas J., 217–222, May 1994..
- [4] Bonner, M., Botts, T., McBreen, J., Mezzina, A., Salzano, F., and Yang, C., Status of advanced electrolytic hydrogen production in the United States and Abroad, Int. J. Hydrogen Energy, 9(4), 269–275, 1984..
- [5] Dutta, S., Technology assessment of advanced electrolytic hydrogen production, Int. J. Hydrogen Energy, 15(6), 379–386, 1990..
- [6] Wendt, H., Water splitting methods, in C.-J. Winter and J. Nitsch (eds.), Hydrogen as an Energy Carrier, Springer-Verlag, Berlin/Heidelberg, Germany, pp. 166–238, 1988..
- [7] Engels, H. et al., Thermochemical hydrogen production, Int. J. Hydrogen Energy, 12(5), 291–295, 1987..
- [8] Yalcin, S., A review of nuclear hydrogen production, Int. J. Hydrogen Energy, 14(8), 551–561, 1989..
- [9] Handbook of Hydrogen Energy EditEd by S.A. Sherif D. Yogi GoswamiElias K. Stefanakos Aldo Steinfeld.
- [10] Bull, S.R., Hydrogen production by photoprocesses, Proceedings of International Renewable Energy Conference, Honolulu, HI, pp. 413–426, 1988..
- [11] Willner, I. and Steinberger-Willner, B., Solar hydrogen production through photobiological, photochemical and photoelectrochemical assemblies, Int. J. Hydrogen Energy, 13(10), 593–604, 1988..
- [12] National Hydrogen Association, The hydrogen technology assessment, phase I. A report for NASA, Washington, DC, 1991..

- [13] "Taylor, J.B., Alderson, J.E.A., Kalyanam, K.M., Lyle, A.B., and Phillips, L.A. Technical and economic assessment of methods for the storage of large quantities of hydrogen, Int. J. Hydrogen Energy, 11(1), 5–22, 1986.".
- [14] "Pottier, J.D. and Blondin, E., Mass storage of hydrogen, in Y. Yurum (ed.), Hydrogen Energy System: Production and Utilization of Hydrogen and Future Aspects, NATO ASI Series E-295, Kluwer Academic Publishers, Dordrecht, the Netherlands, pp. 167–180, 1995".
- [15] "Mitlitsky, F., Development of an advanced, composite, lightweight, high pressure storage tank for on-board storage of compressed hydrogen, Proceedings of the Fuel Cells for Transportation TOPTEC: Addressing the Fuel Infrastructure Issue, Alexandria, VA, S".
- [16] "Brewer, G.D., The prospects for liquid hydrogen fueled aircraft, Int. J. Hydrogen Energy, 7, 21–41, 1982.".
- [17] "Winter, C.J. and Nitsch, J., Hydrogen as an Energy Carrier, Springer-Verlag, Berlin, Germany, 1988.".
- [18] "Veziroglu, T.N., Hydrogen technology for energy needs of human settlements, Int. J. Hydrogen Energy, 12(2), 99–129, 1987.".
- [19] SpringerBriefs in Applied Sciences Ali Salehabadi Mardiana Idayu Ahmad •Norli Ismail
 Norhashimah Morad •Morteza Enhessari.
- [20] M. de Y. Alicia, Y. Oumellal, C. Zlotea, L. Vidal, M.G. Camelia, In-situ Pd–Pt nanoalloys growth in confined carbon spaces and their interactions with hydrogen. Nano-Struct. Nano-Objects 9,1_12(2017).
- [21] G.E. Froudakis, Hydrogen storage in nanotubes&nanostructures. Mater.Today 14, 324–328 (2011)..
- [22] Shafiee, S.; McCay, M.H. Different Reactor and Heat Exchanger Configurations for Metal Hydride Hydrogen Storage Systems—A Review. Int. J. Hydrogen Energy 2016, 41, 9462–9470.
- [23] Kukkapalli, V.K.; Kim, S.; Thomas, S.A. Thermal Management Techniques in Metal Hydrides for Hydrogen Storage Applications: A Review. Energies 2023, 16, 3444...
- [24] Ho, J.Y.; Leong, K.C.; Wong, T.N. Additively-Manufactured Metallic Porous Lattice Heat Exchangers for Air-Side Heat Transfer Enhancement. Int. J. Heat Mass Transf. 2020, 150, 119262..

- [25] Chekurov, S.; Kajaste, J.; Saari, K.; Kauranne, H.; Pietola, M.; Partanen, J. Additively Manufactured High-Performance Counterflow Heat Exchanger. Prog. Addit. Manuf. 2018, 4, 55–61..
- [26] Ye, Y.; Ding, J.; Wang, W.; Yan, J. The Storage Performance of Metal Hydride Hydrogen Storage Tanks with Reaction Heat Recovery by Phase Change Materials. Appl. Energy 2021, 299, 117255..
- [27] Zhang, J.; Fisher, T.S.; Ramachandran, P.V.; Gore, J.P.; Mudawar, I. A Review of Heat Transfer Issues in Hydrogen Storage Technologies. J. Heat Transf. 2005, 127, 1391–1399..
- [28] Kim, K. Performance of High Power Metal Hydride Reactors. Int. J. Hydrogen Energy 1998, 23, 355–362..
- [29] Kim, K.J.; Lloyd, G.; Razani, A.; Feldman, K.T. Development of LaNi5/Cu/Sn Metal Hydride Powder Composites. Powder Technol. 1998, 99, 40–45..
- [30] Bai, X.S.; Yang, W.W.; Zhang, W.Y.; Yang, F.S.; Tang, X.Y. Hydrogen Absorption

 Performance of a Novel Cylindrical MH Reactor with Combined Loop-Type Finned Tube
 and Cooling Jacket Heat Exchanger. Int. J. Hydrogen Energy 2020, 45, 28100–28115...
- [31] Sunku Prasad, J.; Muthukumar, P. Design and Performance Analysis of an Annular Metal Hydride Reactor for Large-Scale Hydrogen Storage Applications. Renew. Energy 2022, 181, 1155–1166..
- [32] Muthukumar, P.; Prakashmaiya, M.; Murthy, S. Experiments on a Metal Hydride-Based Hydrogen Storage Device. Int. J. Hydrogen Energy 2005, 30, 1569–1581..
- [33] Gupta, S.; Sharma, V.K. Design and Analysis of Metal Hydride Reactor Embedded with Internal Copper Fins and External Water Cooling. Int. J. Energy Res. 2020, 45, 1836–1856..
- [34] Y. Fukai. The metal-hydrogen system: basic bulk properties: Springer Science & Business Media, 2006..
- [35] Z. Sun, X. Lu, F.M. Nyahuma, N. Yan, J. Xiao, S. Su, et al., Enhancing hydrogen storage properties of MgH2 by transition metals and carbon materials: a brief review, Front. Chem. 8 (2020) 552.
- [36] E.M. Dematteis, N. Berti, F. Cuevas, M. Latroche, M. Baricco, Substitutional effects in TiFe for hydrogen storage: a comprehensive review, Mater. Adv. 2 (8) (2021) 2524–2560,.

- [37] S. Semboshi, N. Masahashi, S. Hanada, Effect of composition on hydrogen absorbing properties in binary TiMn2 based alloys, J. Alloys Compd. 352 (1–2) (2003) 210–217...
- [38] V.K. Sharma, Kumar E. Anil, Effect of measurement parameters on thermodynamic properties of La-based metal hydrides, Int. J. Hydrog. Energy 39 (11) (2014) 5888–5898..
- [39] N.A. Ali, M. Ismail, Modification of NaAlH4 properties using catalysts for solidstate state hydrogen storage: a review, Int. J. Hydrog. Energy 46 (1) (2021) 766–782..
- [40] Herbert C. Brown, Y.M. Choi, S. Narasimhan, Convenient procedure for the conversion of sodium borohydride into lithium borohydride in simple ether solvents, Inorg. Chem. 12 (1981)..
- [41] T. Nakagawa, Inomata A., Aoki H., Miura T. Numerical analysis of heat and mass transfer characteristics in the metal hydride bed. International Journal of Hydrogen Energy. 2000;25(4):339-50..
- [42] A. V. Gusarov, Kovalev E. P. Model of thermal conductivity in powder beds. Physical Review B. 2009;80(2):024202..
- [43] J. Van de Lagemaat, Benkstein Kurt. D., Frank Arthur. J. Relation between particle coordination number and porosity in nanoparticle films: implications to dye-sensitized solar cells. The Journal of Physical Chemistry B. 2001;105(50):12433-6..
- [44] M. Matsushita, Monde M., Mitsutake Y. Experimental formula for estimating porosity in a metal hydride packed bed. International Journal of Hydrogen Energy. 2013;38(17):7056-64..
- [45] T. L. Bergman, Incropera F. P., DeWitt D. P., Lavine A. S. Fundamentals of heat and mass transfer: John Wiley & Sons, 2011..
- [46] S. S. Mohammadshahi, Gould T., Gray E. MacA., Webb C. J. An improved model for metal-hydrogen storage tanks—Part 1: Model development. International Journal of Hydrogen Energy. 2016;41(5):3537-50..
- [47] D.O. Lazarev and K.B. Minko, "Simulation of Hydrogen Desorption Processes in the Metal-Hydride Accumulator-Fuel Cell System," Therm. Eng., vol. 57, no. 14, pp. 1222–1226, 2010..
- [48] U. Mayer, M. Groll, and W. Supper, "Heat and Mass Transfer in Metal Hydride Reaction Beds: Experimental and Theoretical Results", J. Less-Common Met., vol. 131, pp. 235–244, 1987..
- [49] D. Lazarev, V. Artemov, G. Yankov, and K.B. Minko, "Numerical Simulation of Heat and Mass Transfer in Metal Hydride Hydrogen Accumulators of Different Complex Designs,"

- Proceedings of the 14th International Heat Transfer Conference (IHTC14),IHTC14-22561,.
- [50] V.N. Verbetsky, S.P. Malyshenko, S.V. Mitrokhin, V.V. Solovei, and Yu.F. Shmal'ko, "Metal Hydrides: Properties and Practical Applications. Review of the Works in CISCountries," Int. J. Hydrogen Energy, vol. 23, no. 12, pp. 1165–1177, 1998.
- [51] S. S. Mohammadshahi, Gould T., Gray E. MacA., Webb C. J. An improved model for metal-hydrogen storage tanks—Part 1: Model development. International Journal of Hydrogen Energy. 2016;41(5):3537-50..
- [52] J. Ma, Wang Y., Shi S., Yang F., Bao Z., Zhang Z. Optimization of heat transfer device and analysis of heat & mass transfer on the finned multi-tubular metal hydride tank. International Journal of Hydrogen Energy. 2014;39(25):13583-95..
- [53] S. Mellouli, Askri F., Dhaou H., Jemni A., Nasrallah S B. A study of the thermal behavior of a deformable metal-hydride bed. International Journal of Hydrogen Energy. 2016;41(3):1711-24..